KIF26B silencing prevents osseous transdifferentiation of progenitor/stem cells and attenuates ectopic calcification in a murine model

Mingming Yan, PhD[1,2,*], **Xin Duan, PhD**[1,*], **Lei Cai, PhD**[1], **Weili Zhang, PhD**[1], **Matthew J. Silva, PhD**[1], **Robert H. Brophy, MD**[1], **Muhammad Farooq Rai, PhD**[1,3]

[1]Department of Orthopedic Surgery, Musculoskeletal Research Center, Washington University, School of Medicine, St. Louis, MO, United States

[2]Department of Orthopedic Surgery, The Second Xiangya Hospital, Central South University, Changsha, Hunan, China

[3]Department of Cell Biology and Physiology, Washington University, School of Medicine, St. Louis, MO, United States

Abstract

Ectopic calcification is an osteogenic process that leads to the formation of inappropriate bone within intra-articular soft tissues, often in response to injury or surgery. The molecular mechanisms governing this phenotype have yet to be determined. Using a population genetics approach in mice, we identified an association of the kinesin superfamily member 26b (Kif26b) with injury-induced ectopic calcification through quantitative trait locus analysis, consistent with a GWAS that identified KIF26B as a severity locus for ectopic calcification in patients with hip osteoarthritis. Despite these associations of KIF26B with ectopic calcification, its mechanistic role and functional implications have not yet been fully elucidated. Here, we aim to decipher the functional role of KIF26B in osseous and chondrogenic transdifferentiation of human and murine progenitor/stem cells and in a murine model of non-invasive injury-induced intra-articular ectopic calcification. We found that KIF26B ablation via lentivirus-mediated shRNA significantly arrested osteogenesis of progenitor/stem cells and suppressed the expression of typical osteogenic marker genes. Conversely, KIF26B loss-of-function increased chondrogenesis as demonstrated by Safranin-O staining and expression of chondrogenic marker genes. Furthermore, cell function analysis showed that KIF26B knockdown significantly decreased cell viability and proliferation and induced cellular apoptosis along with suppression of cell proliferation and Wnt signaling genes. Mechanistically, loss of osteogenesis was reverted by addition of a Wnt agonist, SKL2001,

demonstrating a role of KIF26B in canonical Wnt/β-catenin signaling. Finally, intra-articular delivery of Kif26b shRNA in B6–129SF2/J mice significantly reduced intra-articular ectopic calcification at 8 weeks after injury compared to mice treated with non-target scrambled shRNA. In summary, these observations suggest that KIF26B plays crucial roles in ectopic bone formation by repressing osteogenesis, but not chondrogenesis, potentially via modulating Wnt/β-catenin signaling. These findings establish KIF26B as a critical determinant of the osteogenic process in pathologic endochondral bone formation and is an actionable target for pharmacotherapy to mitigate ectopic calcification (and heterotopic ossification).

Keywords

KIF26B; ectopic calcification; Wnt/β-catenin signaling; cell proliferation; cell apoptosis

Introduction

The term *ectopic bone*—from the Greek word *ektopos* meaning "away from a place"— is when non-skeletal soft tissues become bone-like [1]. Most often, ectopic or acquired calcification results from osteogenesis following direct injury to a tissue [2–4]. Ectopic calcification as referred to herein appears as multiple intra-articular nodules in the synovium and joint capsule. It can severely affect the joint and is often recalcitrant to therapy. The incidence of ectopic calcification remains unknown but is not rare. Heterotopic ossification, a form of calcification in soft tissues such as muscles and tendons, has been extensively studied in different contexts and for which the molecular mechanisms have been better understood [5–8]. Intra-articular ectopic calcification, however, has not been studied and characterized as well. Although it is thought that the molecular mechanisms that govern physiological calcification of skeletal tissues are akin to those regulating pathological or ectopic calcification of soft tissues [9], clear knowledge gaps still exist when it comes to understanding the etiopathogenesis of ectopic calcification.

We have taken a population genetics approach to identifying genes involved in ectopic calcification using an advanced intercross of two informative mouse strains: LG/J (Large), a healer strain with a high predisposition for developing ectopic calcification, and SM/J (Small), a non-healer strain with low susceptibility for developing ectopic calcification [4,10–13]. We identified 20 quantitative trait loci (QTLs) influencing ectopic bone formation subsequent to knee trauma in the advanced intercross line randomly mated for 44 generations [4]. The high degree of parental line recombination permitted precise single nucleotide polymorphism mapping to sub-centimorgan intervals containing small sets of candidate genes for the causal genetic factors in synovial ectopic bone formation [4]. Within these QTLs, we identified *Kif26b* as a prime candidate related to ectopic calcification. Furthermore, a genome-wide association study of ectopic calcification in patients after total hip arthroplasty for osteoarthritis has identified *KIF26B* as a gene associated with ectopic calcification severity [14].

KIF26B is a member of the kinesin superfamily of proteins, which are involved in the microtubule and ATP-dependent transport of various cargos to a specific destination [15].

Moreover, studies have shown that *Kif26b* controls endothelial cell polarity, which is tied to non-canonical Wnt signaling [16] and its expression is increased as cells differentiate into chondrocytes [17]. More recently, *Kif26b* has been tested for a role in osseous transdifferentiation of mouse myoblasts [14]. Despite its implication in ectopic calcification in mice and patients, the mechanistic role, and functional implications of *KIF26B* have not yet been fully elucidated.

The purpose of the present study was to advance our understanding of the role of KIF26B in ectopic calcification by examining the effects of KIF26B knockdown on osteogenic or chondrogenic transdifferentiation of progenitor cells *in vitro* as well as in an injury-induced ectopic calcification model of anterior cruciate ligament (ACL) rupture in mice. In addition, we gained mechanistic insights to understand the role of *KIF26B* in Wnt signaling and cell processes such as proliferation and apoptosis, and highlight the potential of *KIF26B* as a mechanistic target in the treatment of ectopic calcification and possibly for other forms of pathological bone formation.

Materials and Methods

Ethics statement

Utilization of discarded ACL tissues from patients undergoing ACL reconstruction surgery was approved by the Washington University Institutional Review Board (Protocol No. 201104119). All patients provided a written and signed informed consent prior to operation. Animal experiments described in this manuscript were approved by the Institutional Animal Care and Use Committee of Washington University (Protocol No. 20190113). An overview of the study design is displayed in Fig. 1.

Cell culture

Progenitor cells were derived from human ACL and termed as ACLp cells [18]. ACLp cells were chosen as clinically relevant intra-articular cells that possess characteristics of mesenchymal stromal cells, i.e., they exhibit the potential to become chondrocytes, osteoblasts, and adipocytes after specific induction [19]. Briefly, ACL fragments were collected from patients ($n = 53$) undergoing ACL reconstruction surgery (Table 1) and were transported to the laboratory in sterile sealed containers containing Dulbecco's phosphate-buffered saline (DPBS, Gibco). Fragments were washed twice with DPBS, and further diced into 3–4 mm^3 pieces. Explants were cultured in 6 well-plates containing Dulbecco's Modified Eagle Medium/Nutrient Mixture F-12 (DMEM/F-12, Gibco) with high glucose (4.5 g/L glucose) and 6 mM L-glutamine and supplemented with 10% fetal bovine serum (FBS, Gibco) and 1% penicillin/streptomycin (100 units/mL and 100 μg/mL respectively, Gibco). Cells were allowed to egress from explants for 3 weeks when explants were removed, and cells were grown in standard culture medium and under ordinary culture conditions. At ~80% confluence, cultures were washed with 1× PBS to remove non-adherent materials and then adherent cells were dissociated by exposure to 0.5% trypsin ethylenediaminetetraacetic acid (Thermo Fisher Scientific), living cells were counted using a hemocytometer and trypan blue exclusion dye. In addition, cultures of murine C2C12 (in-house) and C3H10T1/2 cells (a generous gift from Dr. Regis O'Keefe, Washington

University) were established. C2C12 is a mouse-derived myoblast cell line generated by Blau and colleagues [20], as a subclone of the C2 cell line established by Yaffe and Saxel in 1977 [21]). The C3H10T1/2 cell line was first established in 1973 by Reznikoff and colleagues [22] and has been shown to display fibroblastic morphology in cell culture and are functionally akin to mesenchymal stem cells [23]. Both cell types have been shown to undergo osteogenesis upon osteogenic induction [24,25].

Characterization of ACLp cells

In order to characterize ACLp cells, we used immunofluorescent staining for several stromal cell markers using Human Mesenchymal Stem Cell Characterization Kit (EMD Millipore). This kit contains a panel of positive and negative selection markers for the characterization of the mesenchymal stromal cell population. In brief, 3×10^5 ACLp cells were directly seeded on the Nunc Lab-Tek Chamber Slides (Thermo Fisher Scientific) and cultured for 3 days. Slides were blocked in 10% normal donkey serum (NDS) in PBS at room temperature for 2 hours. After draining off the blocking buffer, slides were incubated with the primary antibodies for respective cell surface marker at 1:200 dilution using 2% NDS in PBS. Mouse IGg was used as negative control. Slides were incubated at 4°C overnight followed by 3 times washes with 1× PBS. Donkey anti-mouse secondary antibody was used (ab150105, Abcam) at 1:200 dilution using 2% NDS in PBS. Phalloidin-iFluor 594 (ab176757, Abcam) was used at 1:500 dilution. Slides were incubated at room temperature for 60 minutes. Finally, the slides were rinsed with PBS before being sealed with VECTASHIELD® antifade mounting medium with 4′,6-diamidino-2-phenylindole (DAPI, Vector Laboratories). Images were taken with Zeiss LSM 880 II Airyscan FAST Confocal Microscope (Zeiss). ACLp cells were also tested for their potential to transdifferentiate into osteoblasts and chondrocytes as described in subsequent sections.

Lentivirus construction, production, and purification

The following shRNA sequences were used to target and silence *KIF26B* mRNA in *Homo sapiens* 5'-CTTGGCTCTTCAAGCTCATAACTCGAGTTATGAGCTTGAAGAGCCAAGTTTTT-3' and 5'-ctgacaacctgctcatcttatctcgagataagatgagcaggttgtcagttttt-3' in *Mus musculus*. Sequences were chemically generated by Thermo Fisher Scientific. ShRNA oligonucleotides were annealed and inserted between the *Age*I and *EcoR*I (New England BioLabs) sites of the recombinant lentivirus expression plasmid (pLKO-1-TRC, Addgene). Scrambled shRNA that did not target any known mRNA, was used as a negative control (termed as scrambled shRNA). Accurate insertion of shRNA cassettes was confirmed by restriction mapping and direct DNA sequencing. Recombinant lentiviruses were generated by co-transfecting human embryonic kidney 293T cells (HEK293T, ATCC) with the lentivirus expression plasmid and packaging plasmid. Briefly, 1.5×10^7 HEK293T cells were seeded in a 15-cm dish and cultured overnight in DMEM medium supplemented with 10% FBS, 2 mM L-glutamine and 1% penicillin and streptomycin at 37°C in a cell culture humidified incubator. Lentiviral expression plasmid (10 μg) and package plasmid (pMd2G, 3 μg; psPax2, 9 μg) were pre-mixed in 1 mL Opti-MEM (Gibco) and Lipofectamine 2000 (80 μL, Life Technologies). Following incubation at room temperature for 15 minutes, contents were then added dropwise to HEK293T cells and incubated for another 16 hours. The medium was then

replenished with 25 mL of complete growth medium, and cells were incubated at 37°C for another 48 hours. Next, the culture medium was collected in a syringe and filtered through a 0.45 μm polyethersulfone membrane filter to remove cell debris. Afterwards, 1/3 volume of Lenti-X concentrator (Clontech) was added to the medium and incubated for 1 hour at 4°C. The viral supernatant was concentrated by centrifugation at 1,500 g for 45 minutes to obtain a pellet. The supernatant was removed carefully, and the pellet was resuspended in 250 μL of 1× DPBS without Ca^{++} and Mg^{++}. Titer of the viral particles was estimated by the Lenti-X™ real-time quantitative polymerase chain reaction (RT-qPCR) Titration Kit (TaKaRa Bio) following supplier's protocol and then aliquoted and stored at −80°C until use.

Lentivirus transduction

ACLp cells or C2C12 or C3H10T1/2 cells were seeded in monolayers at a density of $1×10^5$ cells/well in a 12-well plate for 24 hours and then transduced with scrambled shRNA or KIF26B shRNA at a multiplicity of infection (MOI) of 20 using growth medium containing 100 μg/mL protamine sulfate (5 mg/mL protamine sulfate in Opti-MEM medium) for 24 hours. Fresh growth medium containing Puromycin (4 μg/mL, Sigma-Aldrich) was added for 48 hours to select resistant colonies that acquired successful transduction.

Osteogenic differentiation assay

The osteogenesis was induced by using osteogenic induction medium StemPro Osteogenesis Differentiation Kit (Gibco) according to the manufacturer's instructions. This medium is composed of StemPro Osteocyte/Chondrocyte Differentiation Basal Medium and StemPro Osteogenesis Supplement and supplemented with 1% penicillin/streptomycin. In brief, ACLp cells transduced with KIF26B shRNA or scrambled shRNA ACLp were seeded at a density $2×10^5$ cells/well in 12-well plates either in growth medium or in osteogenic induction medium for up to 28 days with fresh medium changed every 3 days to maintain the activity of cells. For osteogenesis of C3H10T1/2 or C2C12 cells, mouse StemXVivo® Osteogenic/Adipogenic Base Media (R&D Systems) and Mouse/Rat StemXVivo® Osteogenic Supplement (R&D Systems) were used according to the manufacturer's protocol. In brief, cells transduced with Kif26b, or scrambled shRNA were seeded in a 12-well plate at a density of $2×10^5$ cells/well with osteogenic differentiation medium for up to 21 days. Fresh medium was changed every other day. The cultured cells were collected on the indicated time points for staining or for RNA and protein extraction.

Assessment of osteogenesis by Alizarin red staining

Alizarin red staining was performed to measure mineral deposition at indicated time points days after osteogenic induction [26]. ACLp cells or C2C12 or C3H10T1/2 cells were washed twice with 1× PBS and fixed in 4% paraformaldehyde (PFA) solution in PBS for 15 minutes at room temperature. After washing 3 times with deionized H2O, cells were stained with 2% Alizarin Red S Staining Kit (pH 4.2, ScienCell™ Research Laboratories) for 30 minutes at room temperature. Then the dye was removed, and cells were washed with deionized H2O at least 3 times. Cell were visualized under light microscope and images were captured using optical EVOS XL Core Imaging System (Thermo Fisher Scientific).

Chondrogenic differentiation assay

To induce chondrogenesis in 3D culture, the pellet culture method was employed. ACLp cells were transduced with scrambled or KIF26B shRNA at an MOI of 20 for 48 hours and then selected with puromycin (5 μg/mL). To prepare pellets, growth medium containing 3×10^5 cells was dispensed into a 15 mL conical polypropylene tube and spun at 200 g for 5 minutes. The growth medium was replaced by chondrogenic medium: high glucose DMEM (Gibco), 1% penicillin/streptomycin (Sigma-Aldrich), 1% insulin-transferrin-selenium Plus Premix (Corning), 100 nM dexamethasone (Sigma-Aldrich), 10 ng/mL TGF-β3 (R&D Systems), 50 μg/mL L-ascorbic acid 2-phosphate (Sigma-Aldrich), and 40 μg/mL L-proline (Sigma-Aldrich). The tubes with pellets were incubated at 37°C under hypoxic condition (2% O_2) for up to 28 days with medium replenished every other day. The lids of the tubes were loosened to facilitate air exchange. For histology, the pellets were fixed in 10% neutral buffered formalin solution for 2 hours, followed by dehydration in serial dilutions of ethyl alcohol (30% → 50% → 70%) for 30 minutes each. Same procedures were repeated to obtain the pellets for total RNA extraction. Images were acquired from the pellets at the same scale using a standard ruler.

Assessment of chondrogenesis by Safranin-O staining

The pellets were embedded in paraffin wax and sections with a thickness of 5 μm were cut from the paraffin block and coated on the glass slide. The sections were deparaffinized with xylazine and ethyl alcohol, and hydrated in distilled water. Sections were first stained with Weigert's iron hematoxylin working solution for 10 minutes. After washing in running tap water for 10 minutes, sections were the stained with 0.1% aqueous fast green solution for 5 minutes. Sections were rinsed quickly with 1% acetic acid solution for no more than 15 seconds. Next, to visualize glycosaminoglycan, sections were stained with 0.1% aqueous Safranin-O solution for 5 minutes resulting in orange/red staining of negatively charged glycosaminoglycans. Finally, the sections were dehydrated and cleared with 95% ethyl alcohol, absolute ethyl alcohol, and xylene, using 2 changes each, 2 minutes each, cover slipped and imaged using NanoZoomer (Hamamatsu).

RNA isolation and RT-qPCR

Total RNA was extracted from the cells or pellets using RNeasy Mini Kit (Qiagen), according to the manufacturer's instructions [18]. The amount and quality of RNA was measured by Nanodrop spectrophotometer (NanoDrop 2000). The isolated RNA samples were retrotranscribed with a High-Capacity cDNA Reverse Transcription Kit (Thermo Fisher Scientific) to synthesize first strand of single-stranded cDNA [18]. Briefly, reaction containing 1 μg RNA, reaction buffer, dNTP, random primers, and transcriptase was incubated at 25°C for 10 minutes, followed by 37°C for 2 hours and finally at 85°C for 5 minutes. The cDNA was stored at −20°C for future use. To determine the expression of target genes, RT-qPCR was performed using standard methods. 20 μL of reaction mix containing 10 μL of SYBR Green Real-Time PCR Master Mix (Thermo Fisher Scientific), 1 μL cDNA, and 200 nM of gene-specific forward/reverse primer sets. Sequences for forward/reverse primers are shown in Table 2. RT-qPCR was performed on a 7500 Fast Real-time PCR System (Applied Biosystems). The relative expression levels of target genes

were normalized to the amount of *PPIA* expressed. The relative mRNA expression between groups was calculated using $2^{-\Delta\Delta Ct}$ method.

Western blot analysis

Total cells lysates for the protein analysis were prepared by radioimmunoprecipitation assay buffer (Abcam) containing 50 mM Tris-HCl (pH 8.0), 150 mM NaCl, 1% Triton-X-100, 0.1% SDS, 0.5% sodium deoxycholate, and supplemented with $1\times$ complete protease inhibitor cocktail (Millipore Sigma). Total protein concentration was analyzed using Bradford Protein Assay (Bio-Rad). Protein was fractioned in a precast polyacrylamide gel and transferred to polyvinylidene fluoride or polyvinylidene difluoride membrane. Odyssey Blocking buffer (LI-COR Biosciences) containing 0.1% Tween 20 was used to block the protein-containing membranes for 1 hour at room temperature. The membranes were probed with specific primary antibody diluted with Odyssey Blocking buffer overnight at 4°C. The following primary antibodies were used: anti-active β-catenin (8814; Cell Signaling Technology); anti-total-β-catenin (ab16051, Abcam), anti-KIF26B (17422-1-AP, Proteintech) at a 1:1000 dilution and β-actin (A2228; Sigma-Aldrich) at 1:4000 dilution. Secondary antibodies from LI-COR (IRDye® 800CW-labeled anti-rabbit; IRDye® 680RD-labeled anti-mouse) were applied at 1:20000 dilution for 50 minutes at room temperature. Membranes were scanned by LI-COR Odyssey Imager (LI-COR Biosciences) at medium resolution using LI-COR software (RRID: SCR_014579).

Detection of cell proliferation by CCK-8 assay

The numbers of living ACLp cells were measured in a proliferation assay using a Cell Counting Kit 8 (CCK-8, Sigma-Aldrich) according to the supplier's protocol. Briefly, ACLp cells were plated in a 96-well plate at a density of 1×10^3 cells/well. After transduction with scrambled shRNA or KIF26B shRNA for 24 hours, the cells were cultured for indicated time points (0, 3, 5 and 7 days). In CCK-8 assay, 100 μL growth medium with 10 μL of CCK-8 solution was added to each well and the plate was incubated at 37°C for 2 hours. Finally, the absorbance of each well was measured at 450 nm wavelength using BioTek Cytation 5 (BioTek Instruments).

5-ethynyl-2′-deoxyuridine (EdU) incorporation assay

Proliferation of ACLp was evaluated by using Click-iT™ EdU Imaging Kit (Invitrogen) according to the supplier's protocol. Briefly, cells were seeded in a 24-well plate at a density of 1×10^4 cells/well and transduced with scrambled shRNA or KIF26B shRNA. Following culture for 48 hours, cells were exposed to 10 μM EdU reagent for 2 hours then fixed with 4% PFA, permeabilized with 0.5% Triton X-100, and stained with Click-IT reaction cocktail. The cell nuclei were marked with Hoechst 33342 (Invitrogen) at a concentration of 5 μg/mL for 30 minutes. The ratio of EdU positive cells to total cells was calculated under high magnification field using Axio Observer Fluorescence microscope (Zeiss).

Terminal deoxynucleotidyl transferase mediated dUTP nick-end labelling (TUNEL) assay

ACLp cells apoptosis was measured by TUNEL assay using In Situ Cell Death Detection Kit, Fluorescein (Roche) according to the manufacture's protocol. Briefly, 5×10^4 cells were

seeded in a 24-well culture plate and transduced with either KIF26B shRNA or scrambled shRNA for 3 days. Cells were then washed 3 times with $1\times$ PBS and fixed with 4% PFA and permeabilized with 0.1% Triton X-100. The TUNEL reaction mixture was prepared with label solution and enzyme solution at a ratio of 1:9. The cells were incubated with TUNEL reaction mixture at 37°C for 1 hour, followed by Hoechst 33342 staining to identify the nuclei. The samples were visualized with Axio Observer fluorescence microscope (Zeiss). The percentage of TUNEL positive cells in 4 microscopic fields was calculated for quantification purpose using this formula: number of dead cells ÷ total number of cells × 100.

Treatment of ACLp cells with Wnt agonist

To demonstrate whether Wnt/β-catenin pathway improves osteogenic differentiation of ACLp cells that was inhibited by KIF26B knockdown, we treated ACLp cells with the Wnt signaling agonist II SKL2001 (EMD Millipore), a small molecule activator of Wnt/β-catenin pathway [27]. In short, 5×10^5 ACLp cells were first treated with KIF26B shRNA or scrambled shRNA for 48 hours and selected by Puromycin for another 48 hours. Afterwards, 2×10^5 ACLp cells were seeded in 12-well plate. Next osteogenesis was induced as above but in addition, SKL2001 (10 μM) dissolved in dimethyl sulfoxide (DMSO, Sigma-Aldrich) or DMSO only (vehicle) was added to cells. The medium was changed 3 times a week. After 7 days of osteogenic induction, the protein levels of active and total β-catenin were detected by Western blot as described above. After culture for 28 days, the Alizarin red staining was performed as above. After 28 days of osteogenic induction, RNA was isolated and expression of *AXIN2* and *WNT16* was measured using standard methods detailed above.

Murine model of intra-articular ectopic calcification

B6–129SF2/J mice were purchased from The Jackson Laboratory (Stock No. 101045/J). Mice were kept at institution's animal facility with a constant humidity of 30–70%, temperature of 21±1°C, light/dark cycle of 12 hours and high standards of animal husbandry. Experiments were performed on 10-week-old male mice under general anesthesia (2.5% isoflurane in 4 L/minute oxygen). Animals received an intra-articular injection 24 hours before loading and then once fortnightly for up to 8 weeks using a previously described method [28]. Mice either received 10 μL lentivirus Kif26b shRNA (treatment group, $n = 8$), or same volume of lentivirus scrambled shRNA (control group, $n = 7$). Ectopic calcification was instigated in the knee using a non-invasive ACL rupture model [2,29]. Briefly, axial compression was applied through the foot joint via the upper loading cup of a material testing machine (Instron ElectroPuls E1000), while the lower cup held the knee in a fixed position and connected to the load cell. Cyclic load was applied for 0.34 seconds, with a rise and fall time each of 0.17 seconds and a baseline hold time of 10 seconds between each cycle. Highest loading force used was 12 Newtons with a 0.5 Newtons preload force to maintain the limb in fixed position between periods of peak loading. This loading pattern was repeated 60 times in a single loading session. The contralateral left limb served as a control. After recovery from anesthesia, mice resumed prior cage activity with ad libitum food and water intake. At 8 weeks post-injury, mice were sacrificed in a carbon dioxide chamber. Knee joints were separated from the body and skin and soft tissues were removed. Joints were fixed in 10% neutral buffered saline for 48h. Following washing with $1\times$ PBS,

samples were infiltrated in 30% sucrose and kept in 4°C for a week for micro-computed tomography (μCT) scanning.

μCT analysis

Two mice in each group were scanned by *in vivo* μCT using a vivaCT-40 μCT scanner (Scanco-Medical) at 4 weeks after loading to examine the development of ectopic calcification. We noted increased mortality following *in vivo* μCT imaging, therefore, we restricted our analysis of ectopic nodules to *ex vivo* imaging only and present examples of *in vivo* imaging as illustrative information. *Ex vivo* μCT of all mice was used to detect ectopic calcification in mouse knee at 8 weeks after loading. Ossified nodules were visualized by constructing 3-dimensional images in Dragonfly imaging software (Object Research Systems), and were quantified by calculating all mineralized areas in and around the joint space excluding the patella, anterior horns of the menisci and fabella. All analyses were carried out in a blinded fashion. To determine any off-target effects of Kif26b knockdown on pre-existing bone, we measured a number of trabecular and subchondral bone parameters. The following μCT settings were used as described previously [2]: energy = 45 kV, voxel size = 21 μm, intensity = 177 μA and integration time = 300 ms. The following morphometric parameters of the tibial cancellous bone were calculated for trabecular epiphyseal compartments: trabecular bone volume fraction (BV/TV), trabecular thickness (Tb.Th), trabecular separation (Tb.Sp), volumetric bone mineral density (vBMD) and tissue mineral density (TMD). Subchondral bone thickness was measured using a custom-written MATLAB 2015b program (MathWorks).

Histology and confocal microscopy

Undecalcified hind limbs were fresh frozen and sectioned at 5 μm thickness using a cryostat, and stained with Safranin-O as described above. The sections were imaged using NanoZoomer digital slide scanner (Hamamatsu). To confirm the knockdown of Kif26b *in vivo*, we performed immunofluorescent staining. For immunofluorescence, sections were washed with $1\times$ PBS three times. Antigen retrieval was accomplished with 10 μg/mL proteinase K (EMD Millipore) in 10 m*M* Tris-HCl (pH 7.4–8.0) for 20 minutes at 37°C. Non-specific binding was then blocked with 10% goat serum for 1 hour at room temperature. Slides were incubated with rabbit anti-Kif26b (1:50, 17422–1-AP, Proteintech) and rat anti-type II collagen (in house, 1:200) in 2% goat serum overnight at 4°C in a humidified chamber. Antigens were detected by Alexa Fluor® 488 conjugated goat anti-rabbit polyclonal antibody (1:200, ab150077, Abcam) and Alexa Fluor® 594 conjugated goat anti-rabbit polyclonal antibody (1:200, ab150080, Abcam) for 1 hour at room temperature. After another wash, slides were counterstained with Fluoro-Gel II with DAPI. Images were taken with Confocal Laser Scanning Microscope (Leica).

Statistical analyses

Each experiment was performed at least three times in independent patient samples and each assay included at minimum three technical replicates. Images are shown from representative experiments and numeric data are expressed as mean ± standard deviation from all experiments to display the variability across different experiments. Descriptive statistics were used to report group means and standard deviations for numerical data reported in the

text. Quantitative data are shown in the form of box plots with minimum and maximum values and each individual data point unless displayed otherwise. Data were analyzed with the use of GraphPad PRISM ver. 9 (GraphPad Software). A two-tailed Unpaired t-test or Mann-Whitney test was used for comparison between two groups. Kruskal-Wallis test with Dunn's multiple comparison test was used for comparison between more than two groups. For normally distributed data, 1-way analysis of variance with Tukey's post hoc test was used. Two-way analysis of variance test was used for human cell proliferation assay, some chondrogenic expression data, and for mouse trabecular and subchondral bone parameters using Šídák's multiple comparison test when the interaction was significant. The criterion of statistical significance was set at a $p < 0.05$ for all analyses.

Results

Lentivirus-shRNA successfully knocks down *KIF26B* mRNA and protein

KIF26B expression in human ACLp cells and murine C3H10T1/2 and C2C12 cells was ablated via lentivirus-mediated shRNA targeting *KIF26B* (Fig. 2A–B). *KIF26B* mRNA expression as measured by RT-qPCR was effectively inhibited to about 80% after KIF26B shRNA transduction compared to scrambled shRNA transduction (0.21±0.03 vs. 1.01±0.14; $p < 0.001$) (Fig. 2C). The data from RT-qPCR paralleled Western blot findings. KIF26B protein production as detected by Western blot analysis was also decreased significantly by KIF26B shRNA compared to scrambled shRNA (0.24±0.10 vs. 1.00±0.00; $p < 0.001$) (Fig. 2D–E). Similar to human ACLp cells, we also knocked down the expression of Kif26b in murine C3H10T1/2 and C2C12 cells. RT-qPCR analysis showed decreased *Kif26b* mRNA in C3H10T1/2 cells transduced with Kif26b shRNA compared to those transduced with scrambled shRNA (0.55±0.03 vs. 1.02±0.22; $p = 0.005$) (Fig. 2F). In C2C12 cells, the expression of *Kif26b* mRNA was lower in cells transduced with Kif26b shRNA than cells transduced with scrambled shRNA (0.37±0.07 vs. 1.02±0.06; $p < 0.001$) (Fig. 2G). These observations indicate that KIF26B shRNA transduction successfully suppressed expression of KIF26B both at mRNA and protein levels *in vitro*.

ACLp cells express stromal cell markers and undergo osteoblastic differentiation *in vitro*

The cells that migrate out of human ACL tissues constitute a rich population of progenitor cells that exhibit stromal cell like properties and have the ability to transdifferentiate into chondrocytes, osteoblasts, and fat cells [19]. We observed that cells begin to migrate out of the tissues within a few days, and over a period of 3 weeks the culture plates became confluent (Supplementary Fig. 1A). Prior to testing the effect of *KIF26B* knockdown on ACLp cells transdifferentiation, we tested these cells for stromal cell markers and osteogenic differentiation potential. Immunostaining revealed that ACLp cells showed positive staining for CD44, CD90, CD146 and Stro-1, but negative for CD14 and CD19 (Supplementary Fig. 1B). Next, we showed that ACLp cells differentiated into osteoblasts when induced by osteogenic medium over a period of 28 days (Supplementary Fig. 1C). We also observed that ACLp cells after osteogenic induction displayed significant increase in the osteogenic marker, *ALPL* compared with the cells in growth medium (13.04±6.33 vs. 1.08±0.52; $p = 0.001$) (Supplementary Fig. 1D).

KIF26B knockdown attenuates osteogenesis

To determine whether KIF26B knockdown significantly decreases osteogenic differentiation of ACLp cells, we transduced ACLp cells with KIF26B shRNA or scrambled shRNA in osteogenic medium for 28 days. Culture with osteogenic induction media significantly increased osteogenesis in control and scrambled shRNA groups compared with ACLp cells cultured in growth medium (data not shown). *KIF26B* knockdown significantly arrested osseous transdifferentiation of ACLp cells compared to scrambled shRNA (Fig. 3A). To further confirm these findings, we measured the expression of typical osteogenic markers showing that the expression of *RUNX2* (0.42 ± 0.01 vs. 1.00 ± 0.01; $p < 0.001$), *ALPL* (0.68 ± 0.02 vs. 1.06 ± 0.06; $p < 0.001$), and *BGLAP* (0.56 ± 0.04 vs. 0.88 ± 0.11; $p < 0.001$) was decreased in ACLp cells receiving KIF26B shRNA compared with those receiving scrambled shRNA (Fig. 3B–D). These findings suggests that KIF26B is required for osteogenic transdifferentiation of ACLp cells since its ablation significantly arrests this process.

We also tested the functional role of Kif26b in two murine cell types: C3H10T1/2 cells and C2C12 cells. We found that Kif26b knockdown significantly suppressed osteogenesis of C3H10T1/2 cells compared to scrambled shRNA (Fig. 4A). Likewise, we found that knockdown of Kif26b significantly arrested osseous transdifferentiation of C2C12 cells as evidenced by loss of Alizarin red staining (Fig. 4B). This observation was further supported by decreased expression of osteogenic-specific marker genes *Runx2* (0.71 ± 0.04 vs. 0.92 ± 0.07; $p = 0.010$) (Fig. 4C), *Alpl* (0.64 ± 0.02 vs. 0.99 ± 0.10; $p = 0.004$) (Fig. 4D), *Bglap* (0.85 ± 0.03 vs. 0.96 ± 0.03; $p = 0.011$) (Fig. 4E), as well as the expression of *Axin2* (0.64 ± 0.04 vs. 0.95 ± 0.03; $p < 0.001$) (Fig. 4F), a downstream target of Wnt/β-catenin signaling.

KIF26B loss-of-function promotes chondrogenesis

To determine whether KIF26B knockdown affects chondrogenic differentiation of ACLp cells, we transduced ACLp cells with KIF26B shRNA or scrambled shRNA in chondrogenic medium for 28 days. The expression of *KIF26B* mRNA was still significantly less in pellets prepared from cells transduced with KIF26B shRNA ($n = 4$) than scrambled shRNA ($n = 3$) (0.62 ± 0.13 vs. 1.01 ± 0.13; $p = 0.011$) after 28 days of chondrogenesis, indicating that KIF26B expression was successfully suppressed during the chondrogenesis (Fig. 5A). We then measured the expression of typical chondrogenic-specific marker genes showing a significant treatment (KIF26B shRNA, scrambled shRNA) by condition (growth medium, chondrogenic medium) interaction for *SOX9* ($P < 0.001$) (Fig. 5B), *COL2A1* ($p = 0.018$) (Fig. 5C), and *ACAN* ($p < 0.001$) (Fig. 5D), with increased expression of these markers in ACLp cells transduced with KIF26B shRNA compared with those transduced with scrambled shRNA. The expression of *AXIN2* (0.46 ± 0.05 vs. 1.00 ± 0.96; $p < 0.001$) was decreased in cells transduced with KIF26B shRNA than scrambled shRNA (Fig. 5E). The pellet size was slightly smaller in KIF26B shRNA group than scrambled shRNA group (Fig. 5F). Cartilage matrix deposition was measured by histological examination of glycosaminoglycan by Safranin-O staining. The intensity of Safranin-O staining was very high (indicative of rich proteoglycan contents) in pellets in KIF26B shRNA group in contrast to scrambled shRNA group where the intensity was notably low (Fig. 5G). We also

noted more homogeneous chondrocytes, as demonstrated by Safranin-O staining, in KIF26B shRNA group than scrambled shRNA group. Together, these findings highlight a positive role of KIF26B knockdown on chondrogenic transdifferentiation of ACLp cells.

Loss of KIF26B attenuates cell proliferation

To elucidate the effects of KIF26B knockdown on cell proliferation, we examined number of living ACLp cells in KIF26B shRNA group. Using CCK-8 assay, we showed that cells treated with KIF26B shRNA exhibited significantly less numbers at day 3, day 5 and day 7 time points compared to both cells treated with scrambled shRNA and non-treated control cells (Fig. 6A). At day 1, we observed no significant differences in cell number across groups. At day 3, cell number was significantly lower in the *KIF26B* shRNA group compared to both control ($p = 0.007$) and scrambled shRNA ($p = 0.033$) groups. Similarly, at day 5 and 7, cell number was significantly lower in KIF26B shRNA transduced cells compared to untreated control ($p < 0.001$; $p < 0.001$) and cells transduced with scrambled shRNA ($p = 0.002$; $p = 0.001$).

We then performed EdU staining to gauge the effects of *KIF26B* knockdown on cell proliferation. Results showed that number of EdU positive cells were less in KIF26B shRNA transduced group than scrambled shRNA and control groups (Fig. 6B). The number of EdU positive cells was also significantly different across groups (1-way ANOVA $p = 0.012$, F = 10.27). Specifically, there were significantly lower EdU positive cells in the KIF26B shRNA (8.00±2.65) group compared to control (19.33±4.93; $p = 0.047$) and scrambled shRNA (24.00±5.29; $p = 0.011$) groups (Fig. 6C). Finally, we showed that mRNA expression of various cell proliferation markers such as *PCNA* (Kruskal-Wallis $p < 0.001$) and *XRCC2* (Kruskal-Wallis $p < 0.001$) was significantly lower in cells treated with KIF26B shRNA as shown in Fig. 6D. Specifically, we observed that the expression of *PCNA* was significantly lower in the KIF26B shRNA (0.67±0.15) group compared to control (1.00±0.00; $p = 0.010$) and scrambled shRNA (0.96±0.10; $p = 0.014$) groups. Similarly, the expression of *XRCC2* was significantly lower in the KIF26B shRNA (0.63±0.08) group compared to control (1.00±0.00; $p = 0.003$) and scrambled shRNA (1.02±0.08; $p = 0.025$) groups.

Loss of *KIF26B* induces cellular apoptosis

Recognizing that *KIF26B* loss-of-function attenuates cell proliferation, we tested whether *KIF26B* knockdown influences cellular apoptosis. Cells treated with KIF26B shRNA showed increased number of TUNEL positive cells (Fig. 7A). Quantification further showed that fraction of TUNEL positive cells was significantly higher in the KIF26B shRNA group compared to the scrambled shRNA group (4.65±0.62 vs. 0.79±0.32; $p < 0.001$) (Fig. 7B). In addition, we also measured the expression of genes related to cellular apoptosis. We observed that the expression of pro-apoptotic *BAX* mRNA was significantly increased in cells treated with KIF26B shRNA compared with cells treated with scrambled shRNA (3.31±0.35 vs. 0.97±0.08; $p < 0.001$) (Fig. 7C). At the same time, the expression of anti-apoptotic gene, *BCL2*, was significantly decreased in cells treated with KIF26B shRNA compared with scrambled shRNA (0.46±0.01 vs. 1.02±0.05; $p < 0.001$) (Fig. 7D). The net ratio of *BAX* and *BCL2* (*BAX/BCL2*), which is an indicator of apoptosis, was significantly

increased in cells treated with KIF26B shRNA compared to those treated with scrambled shRNA (7.29±0.80 vs. 0.95±0.08; $p < 0.001$) (Fig. 7E).

KIF26B modulates Wnt/β-catenin signaling

We next tested whether *KIF26B* knockdown influences canonical Wnt/β-catenin signaling. We observed that knockdown of *KIF26B* suppressed the expression of Wnt/β-catenin pathway as demonstrated by the decrease in mRNA expression of *WNT16* (0.70±0.02 vs. 1.00±0.11; $p < 0.001$) (Fig. 8A) and *AXIN2* (0.97±0.03 vs. 0.63±0.04; $p < 0.001$) (Fig. 8B), mRNA compared to scrambled shRNA. These findings are supported by a decrease in the protein level of active β-catenin (0.47±0.13 vs. 1.00±0.00; $p < 0.001$) and total β-catenin (0.55±0.21 vs. 1.00±0.00; $p = 0.005$) in KIF26B shRNA cells compared to scrambled shRNA transduced cells (Fig. 8C–E). Together, these data suggest that *KIF26B* modulates the expression of canonical Wnt/β-catenin signaling.

Next, we used Wnt agonist II, SKL2001, to test whether it rescues the lost phenotype. We first showed that compared with vehicle (DMSO), the expression of Wnt/β-catenin signaling genes, namely *WNT16* (3.06±0.13 vs. 1.00±0.14; $p < 0.001$) (Fig. 9A) and *AXIN2* (2.20±0.08 vs. 1.00±0.02; $p < 0.001$) (Fig. 9B), was increased in SKL2001 treated cells. Our findings further demonstrate that decrease in osteogenesis due to *KIF26B* loss-of-function was reverted by the addition of Wnt agonist II (Fig. 9C). Consistently, the protein levels of active β-catenin were decreased after *KIF26B* knockdown, which was significantly attenuated by SKL2001 treatment (Fig. 9D). Quantification of Western blot signal intensity was in parallel to these observations both for active β-catenin (1-way ANOVA $p < 0.001$, F = 20.75) (Fig. 9E) and total β-catenin (1-way ANOVA $p < 0.001$, F = 53.18) (Fig. 9F).

Based on these observations, our working model displayed in Fig. 10 shows that KIF26B inhibition decreases total β-catenin and active β-catenin levels and results in suppression of osteogenesis of ACLp cells coupled with the inhibition of typical osteogenic-specific marker genes. Moreover, KIF26B silencing promotes the chondrogenic differentiation of ACLp cells and stimulates the expression of chondrogenic-specific markers.

Kif26b shRNA treatment suppresses Kif26b expression and mitigates ectopic calcification in mice

Whereas increased Kif26b staining was noted in knees treated with scrambled shRNA, the staining intensity of Kif26b in Kif26b shRNA treatment group was minimal indicating that Kif26b shRNA administration effectively suppressed the expression of Kif26b protein *in vivo* (Fig. 11A). Since KIF26B knockdown promoted chondrogenesis in vitro, we measured proteoglycan in ectopic calcified nodules. We found that there was an increased Safranin O staining intensity in the Kif26b shRNA group compared with the scrambled shRNA group indicating increased chondrogenesis (Fig. 11A). In order to investigate the role of *Kif26b* in ectopic calcification, we applied an injury-induced ectopic calcification model in mice. We showed that intra-articular delivery of Kif26b shRNA did not reduce the number of calcified nodules at 4 weeks after injury as determined by *in vivo* μCT analysis (Supplementary Fig. 2). However, at 8 weeks, we observed fewer nodules in *Kif26b* knockdown group (Fig. 11B). Quantification of nodules showed that the number of nodules significant decreased

in in mice receiving Kif26b shRNA compared with scrambled shRNA (4.00±0.71 vs. 7.25±0.96; $p < 0.001$) (Fig. 11C).

Kif26b shRNA does not affect pre-existing trabecular and subchondral bone

We also measured the effect of Kif26b knockdown on already formed bone cancellous bone in the proximal tibia. We found that Kif26b knockdown did not significantly affect trabecular bone parameters namely BV/TV ($p = 0.883$), Tb.Th ($p = 0.167$), Tb.Sp ($p = 0.795$), vBMD ($p = 0.855$), and TMD ($p = 0.836$), nor did it affect subchondral bone plate thickness ($p = 0.645$) (Supplementary Fig. 3).

Discussion

These findings establish *KIF26B* as a critical participant in the osteogenic process and a viable pharmacotherapy target for the treatment of pathologic ectopic calcification. In conjunction with the findings of Hatzkotoulas and colleagues [14], these results suggest that *KIF26B* plays a role in ectopic calcification which is target for biologic treatments to treat and potentially prevent the development of ectopic calcification. These findings are clinically significant as there are currently no biological treatment options available to prevent or treat the development of ectopic calcification. Although surgical excision of ossified nodules from the joint is indicated in severe cases where calcified nodules impede joint movement [30], the recurrence rate is very high [31]. Unlike osteophytes, which are attached to the bone surface, ectopic calcified nodules are embedded in the joint capsule and/or in the synovium. In addition, while these nodules are relatively benign when embedded in soft issues (e.g., synovium or joint capsule), they can become loose in the joint and put patients at risk for mechanical symptoms and damage to the articular cartilage. Our interest in KIF26B developed from a previous large scale genetic screening of several advanced intercross mouse lines for the development of trauma-induced ectopic calcification, in which we identified *Kif26b* as a prime candidate gene implicated in ectopic calcification [4]. A recent genome-wide association study in human cases of hip ossification identified *KIF26B* as a severity locus for pathological bone formation [14], independently verifying our finding in mice. These studies establish *KIF26B* on the leading edge of research into intra-articular ectopic calcification.

A recent study by Hatzkotoulas and colleagues [14] showed that *KIF26B* is expressed in bone and that modulation of *KIF26B* in an *in vitro* model of murine myoblast osteogenesis is able to inhibit osseous transdifferentiation of C2C12 cells. This effect is mechanistically driven through ERK1/2 signaling. A novel finding of our study is that *KIF26B* affects the canonical Wnt/β-catenin signaling pathway. Previously, it has been reported that *KIF26B* functions via non-canonical Wnt5a-Ror signaling to control morphogenetic cell and tissue behavior [16]. *Kif26b* has also been shown to switch canonical β-catenin–dependent pathway toward the non-canonical PCP pathway [32]. After Wnt3a stimulation, *Kif26b* depletion induces an increase in the ratio between active and total β-catenin, which suggests activation of the canonical Wnt signaling pathway. Nalesso et al. [33] demonstrated that cartilage repair requires a switch in the Wnt pathway mediated by *Wnt16*; this redirects the cell from the canonical pathway to the non-canonical pathway, where a repair pathway characterized by

lubricin is synthesized in place of the canonical *AXIN2*. Although cartilage and bone do not appear on any tissue blots, one study showing enhancer-trap LacZ transgene of *Kif26b* during development demonstrated strong expression in the somites, limb buds, and face in the embryo [34]. In addition, studies of stem cell differentiation showed increases in Kif26b as cells differentiate into chondrocytes [17].

KIF26B also modulated two particularly important cellular processes: cell proliferation and apoptosis. We observed that cells treated with KIF26B shRNA showed impaired viability and proliferation capability compared to control cells. As cell proliferation is associated with increased ossification [35], our observation that *KIF26B* knockdown suppresses cell proliferation and ectopic calcification explains the role of *KIF26B* in modulating ectopic calcification by altering cell function. We surmised that the osteogenic medium would significantly promote proliferation of ACLp cells transduced with KIF26B shRNA, which is different from the effects of KIF26B knockdown on ACLp cells in the context of growth medium. Compared to growth medium, the ingredients in osteogenic medium facilitate cell proliferation and then induce osteogenic differentiation. That may be the reason we did not find massive cell apoptosis after *KIF26B* silencing in ACLp cells during osteogenesis. While there is no direct link known between ectopic calcification and apoptosis, some studies have shown that factors that induce heterotopic ossification such as hypoxia and HIF1α [7] regulate apoptosis [35,36].

In this study, we focused on ligament-derived progenitor cells in contrast to more commonly used mesenchymal progenitor cells, although we have confirmed that KIF26B loss-of-function equally impedes osteogenesis in other cell types such as murine C2C12 and C3H10T1/2 cells. Since ACLp cells express stem cell markers as defined by the International Society of Cellular Therapy and adhere to plastic [37], these cells have translational value for this clinical problem. This approach offers some advantages from clinical and translational perspectives. While heterotopic ossification in tendons and ligaments is not uncommon [38], frequently occurring in inflamed and injured ligaments/tendons which results in disability and pain, its pathogenesis is poorly understood. Calcification in tendons and ligament follows the same endochondral ossification path that is followed by embryonic bone development and ossification of the knee [39,40]. However, our study does not imply that ACLp cells are the sole source of cells that contribute to ectopic calcification in the joint. Several other cell types have been implicated in ectopic bone formation such as immune and stromal cells and CD146+ pericytes [41,42]. In fact, we have previously shown that cells responding to ACL tears in mice originate from the synovium, subchondral bone marrow and Grove of Ranvier [29]. Intra-articular injection of KIF26B shRNA targets all cells within the synovial joint so the therapeutic effect observed in this study is not specific to ACLp cells.

While this study demonstrates that *Kif26b* knockdown suppresses the development of intra-articular ectopic calcification after mechanical trauma and provides some mechanistic insights, many questions remain. For instance, we have shown that Wnt/β-catenin pathway is involved downstream of *KIF26B*, whereas Hatzkotoulas et al., [14] have shown crosstalk between ERK signaling and *KIF26B*. A number of other studies have shown the involvement of other critical genes and pathways in heterotopic ossification, such

as HIF1α [7], TGF-β [40] and BMP-2 [43]. Further research is needed to investigate whether these pathways are linked to *KIF26B* signaling. Thus, it is clear while several genes and pathways participate in this phenotype, ectopic calcification occurs mainly through endochondral bone formation. To this end, we examined the role of KIF26B on chondrogenic differentiation of ACLp cells finding that knockdown of KIF26B instead increased chondrogenesis. It was an interesting observation as it implies that the decrease in ectopic calcification was predominantly through inhibition of osteogenic pathway. This observation also highlights that KIF26B has a dual but opposite effect on endochondral ossification, further investigation is necessary to confirm and better characterize this finding.

While the function of KIF26B on chondrogenesis has not been reported previously, many studies have demonstrated that loss of Wnt signaling exacerbates chondrogenesis [44,45], much of this can be explained by decreased Wnt signaling with KIF26B knockdown in our experiments. Intense Safranin O staining of nodules in Kif26b shRNA treated knees corroborate our findings that KIF26B knockdown increases chondrogenic differentiation of ACLp cells. Additional detailed time-course studies using other techniques such as *in vivo* cell labelling and histology would be necessary to assess when KIF26B affects chondrogenesis and osteogenesis, which were not performed here and constitute a limitation of this work. The role of cellular processes such as proliferation and apoptosis in the development of ectopic calcification are still yet to be determined. Studies with *KIF26B* genetic gain/loss-of-function studies in murine ectopic calcification would be another opportunity to better understand the role of *KIF26B* in ectopic calcification.

In summary, our study explored the effects of *KIF26B* silencing on inhibition of ectopic calcification development *in vitro* and *in vivo* and identified crosstalk between *KIF26B* and canonical Wnt/β-catenin signaling during osteogenic differentiation. These findings demonstrate that inhibition of *KIF26B* is a potential target for interventions to treat ectopic calcification. This study also provides new insights into understanding the mechanism of ectopic calcification, although additional studies are desirable to fully capture the etiopathogenesis of this pathology.

Supplementary Material

Refer to Web version on PubMed Central for supplementary material.

Acknowledgments

Financial supporters

Data availability

The data that support the findings of this study are available from the corresponding author upon reasonable request.

References

1. Scott MA, Levi B, Askarinam A, Nguyen A, Rackohn T, Ting K, et al. Brief review of models of ectopic bone formation. Stem Cells Dev. Mar 20 2012;21(5):655–67.

2. Rai MF, Duan X, Quirk JD, Holguin N, Schmidt EJ, Chinzei N, et al. Post-Traumatic Osteoarthritis in Mice Following Mechanical Injury to the Synovial Joint. Sci Rep. Mar 27 2017;7:45223. Epub 2017/03/28. [PubMed: 28345597]

3. Forsberg JA, Pepek JM, Wagner S, Wilson K, Flint J, Andersen RC, et al. Heterotopic ossification in high-energy wartime extremity injuries: prevalence and risk factors. J Bone Joint Surg Am. May 2009;91(5):1084–91. Epub 2009/05/05. [PubMed: 19411456]

4. Rai MF, Schmidt EJ, Hashimoto S, Cheverud JM, Sandell LJ. Genetic loci that regulate ectopic calcification in response to knee trauma in LG/J by SM/J advanced intercross mice. J Orthop Res. Oct 2015;33(10):1412–23. Epub 2015/05/20. [PubMed: 25989359]

5. Pacifici M Acquired and congenital forms of heterotopic ossification: new pathogenic insights and therapeutic opportunities. Curr Opin Pharmacol. Jun 2018;40:51–8. Epub 2018/04/04. [PubMed: 29614433]

6. Sinha S, Uchibe K, Usami Y, Pacifici M, Iwamoto M. Effectiveness and mode of action of a combination therapy for heterotopic ossification with a retinoid agonist and an anti-inflammatory agent. Bone. Sep 2016;90:59–68. Epub 2016/02/20. [PubMed: 26891836]

7. Agarwal S, Loder S, Brownley C, Cholok D, Mangiavini L, Li J, et al. Inhibition of Hif1alpha prevents both trauma-induced and genetic heterotopic ossification. Proc Natl Acad Sci U S A. Jan 19 2016;113(3):E338–47. Epub 2016/01/02. [PubMed: 26721400]

8. Sorkin M, Huber AK, Hwang C, Carson WFt, Menon R, Li J, et al. Regulation of heterotopic ossification by monocytes in a mouse model of aberrant wound healing. Nat Commun. Feb 5 2020;11(1):722. Epub 2020/02/07. [PubMed: 32024825]

9. Mundy C, Yao L, Sinha S, Chung J, Rux D, Catheline SE, et al. Activin A promotes the development of acquired heterotopic ossification and is an effective target for disease attenuation in mice. Sci Signal. Feb 9 2021;14(669). Epub 2021/02/11.

10. Rai MF, Hashimoto S, Johnson EE, Janiszak KL, Fitzgerald J, Heber-Katz E, et al. Heritability of articular cartilage regeneration and its association with ear wound healing in mice. Arthritis and rheumatism. Jul 2012;64(7):2300–10. Epub 2012/01/26. [PubMed: 22275233]

11. Hashimoto S, Rai MF, Janiszak KL, Cheverud JM, Sandell LJ. Cartilage and bone changes during development of post-traumatic osteoarthritis in selected LGXSM recombinant inbred mice. Osteoarthritis and cartilage. Jun 2012;20(6):562–71. Epub 2012/03/01. [PubMed: 22361237]

12. Rai MF, Schmidt EJ, McAlinden A, Cheverud JM, Sandell LJ. Molecular insight into the association between cartilage regeneration and ear wound healing in genetic mouse models: targeting new genes in regeneration. G3 (Bethesda, Md). Nov 6 2013;3(11):1881–91. Epub 2013/09/05. [PubMed: 24002865]

13. Chinzei N, Rai MF, Hashimoto S, Schmidt EJ, Takebe K, Cheverud JM, et al. Evidence for Genetic Contribution to Variation in Posttraumatic Osteoarthritis in Mice. Arthritis & rheumatology (Hoboken, NJ). Mar 2019;71(3):370–81. Epub 2018/09/19.

14. Hatzikotoulas K, Pickering GAE, Clark MJ, Felix-Ilemhenbhio F, Kocsy K, Simpson J, et al. Genome-wide association and functional analyses identify CASC20 and KIF26B as target loci in heterotopic ossification. bioRxiv. 2019:845958.

15. Miki H, Setou M, Kaneshiro K, Hirokawa N. All kinesin superfamily protein, KIF, genes in mouse and human. Proc Natl Acad Sci U S A. Jun 19 2001;98(13):7004–11. Epub 2001/06/21. [PubMed: 11416179]

16. Susman MW, Karuna EP, Kunz RC, Gujral TS, Cantu AV, Choi SS, et al. Kinesin superfamily protein Kif26b links Wnt5a-Ror signaling to the control of cell and tissue behaviors in vertebrates. Elife. Sep 8 2017;6. Epub 2017/09/09.

17. Huynh NPT, Zhang B, Guilak F. High-depth transcriptomic profiling reveals the temporal gene signature of human mesenchymal stem cells during chondrogenesis. FASEB J. Jan 2019;33(1):358–72. Epub 2018/07/10.

18. Cai L, Brophy RH, Tycksen ED, Duan X, Nunley RM, Rai MF. Distinct expression pattern of periostin splice variants in chondrocytes and ligament progenitor cells. FASEB journal : official publication of the Federation of American Societies for Experimental Biology. Jul 2019;33(7):8386–405. Epub 2019/04/18. [PubMed: 30991832]

19. Steinert AF, Kunz M, Prager P, Barthel T, Jakob F, Noth U, et al. Mesenchymal stem cell characteristics of human anterior cruciate ligament outgrowth cells. Tissue Eng Part A. May 2011;17(9–10):1375–88. Epub 2011/01/21. [PubMed: 21247268]

20. Blau HM, Pavlath GK, Hardeman EC, Chiu CP, Silberstein L, Webster SG, et al. Plasticity of the differentiated state. Science. Nov 15 1985;230(4727):758–66. Epub 1985/11/15. [PubMed: 2414846]

21. Yaffe D, Saxel O. Serial passaging and differentiation of myogenic cells isolated from dystrophic mouse muscle. Nature. Dec 22–29 1977;270(5639):725–7. Epub 1977/12/22. [PubMed: 563524]

22. Reznikoff CA, Brankow DW, Heidelberger C. Establishment and characterization of a cloned line of C3H mouse embryo cells sensitive to postconfluence inhibition of division. Cancer Res. Dec 1973;33(12):3231–8. Epub 1973/12/01. [PubMed: 4357355]

23. Tang QQ, Otto TC, Lane MD. Commitment of C3H10T1/2 pluripotent stem cells to the adipocyte lineage. Proc Natl Acad Sci U S A. Jun 29 2004;101(26):9607–11. Epub 2004/06/24. [PubMed: 15210946]

24. Shea CM, Edgar CM, Einhorn TA, Gerstenfeld LC. BMP treatment of C3H10T1/2 mesenchymal stem cells induces both chondrogenesis and osteogenesis. J Cell Biochem. Dec 15 2003;90(6):1112–27. Epub 2003/11/25. [PubMed: 14635186]

25. Katagiri T, Yamaguchi A, Komaki M, Abe E, Takahashi N, Ikeda T, et al. Bone morphogenetic protein-2 converts the differentiation pathway of C2C12 myoblasts into the osteoblast lineage. J Cell Biol. Dec 1994;127(6 Pt 1):1755–66. Epub 1994/12/01. [PubMed: 7798324]

26. Puchtler H, Meloan SN, Terry MS. On the history and mechanism of alizarin and alizarin red S stains for calcium. J Histochem Cytochem. Feb 1969;17(2):110–24. Epub 1969/02/01. [PubMed: 4179464]

27. Gwak J, Hwang SG, Park HS, Choi SR, Park SH, Kim H, et al. Small molecule-based disruption of the Axin/beta-catenin protein complex regulates mesenchymal stem cell differentiation. Cell Res. Jan 2012;22(1):237–47. Epub 2011/08/10. [PubMed: 21826110]

28. Yan H, Duan X, Pan H, Holguin N, Rai MF, Akk A, et al. Suppression of NF-kappaB activity via nanoparticle-based siRNA delivery alters early cartilage responses to injury. Proc Natl Acad Sci U S A. Oct 11 2016;113(41):E6199–E208. [PubMed: 27681622]

29. Duan X, Rai MF, Holguin N, Silva MJ, Patra D, Liao W, et al. Early changes in the knee of healer and non-healer mice following non-invasive mechanical injury. J Orthop Res. Mar 2017;35(3):524–36. [PubMed: 27591401]

30. van Kuijk AA, Geurts AC, van Kuppevelt HJ. Neurogenic heterotopic ossification in spinal cord injury. Spinal Cord. Jul 2002;40(7):313–26. Epub 2002/06/25. [PubMed: 12080459]

31. Shehab D, Elgazzar AH, Collier BD. Heterotopic ossification. J Nucl Med. Mar 2002;43(3):346–53. Epub 2002/03/09. [PubMed: 11884494]

32. Descamps B, Sewduth R, Ferreira Tojais N, Jaspard B, Reynaud A, Sohet F, et al. Frizzled 4 regulates arterial network organization through noncanonical Wnt/planar cell polarity signaling. Circ Res. Jan 6 2012;110(1):47–58. [PubMed: 22076635]

33. Nalesso G, Thomas BL, Sherwood JC, Yu J, Addimanda O, Eldridge SE, et al. WNT16 antagonises excessive canonical WNT activation and protects cartilage in osteoarthritis. Ann Rheum Dis. Jan 2017;76(1):218–26. [PubMed: 27147711]

34. Marikawa Y, Fujita TC, Alarcon VB. An enhancer-trap LacZ transgene reveals a distinct expression pattern of Kinesin family 26B in mouse embryos. Dev Genes Evol. Feb 2004;214(2):64–71. [PubMed: 14727108]

35. Huang Y, Wang X, Lin H. The hypoxic microenvironment: a driving force for heterotopic ossification progression. Cell Commun Signal. Feb 7 2020;18(1):20. Epub 2020/02/08. [PubMed: 32028956]

36. Bensaid S, Fabre C, Fourneau J, Cieniewski-Bernard C. Impact of different methods of induction of cellular hypoxia: focus on protein homeostasis signaling pathways and morphology of C2C12 skeletal muscle cells differentiated into myotubes. J Physiol Biochem. Aug 2019;75(3):367–77. Epub 2019/07/04. [PubMed: 31267382]

37. Dominici M, Le Blanc K, Mueller I, Slaper-Cortenbach I, Marini F, Krause D, et al. Minimal criteria for defining multipotent mesenchymal stromal cells. The International Society for Cellular Therapy position statement. Cytotherapy. 2006;8(4):315–7. Epub 2006/08/23. [PubMed: 16923606]

38. Zhang Q, Zhou D, Wang H, Tan J. Heterotopic ossification of tendon and ligament. J Cell Mol Med. May 2020;24(10):5428–37. Epub 2020/04/16. [PubMed: 32293797]

39. Sugita D, Yayama T, Uchida K, Kokubo Y, Nakajima H, Yamagishi A, et al. Indian hedgehog signaling promotes chondrocyte differentiation in enchondral ossification in human cervical ossification of the posterior longitudinal ligament. Spine (Phila Pa 1976). Oct 15 2013;38(22):E1388–96. Epub 2013/07/26. [PubMed: 23883825]

40. Wang X, Li F, Xie L, Crane J, Zhen G, Mishina Y, et al. Inhibition of overactive TGF-beta attenuates progression of heterotopic ossification in mice. Nat Commun. Feb 7 2018;9(1):551. Epub 2018/02/09. [PubMed: 29416028]

41. Meyers CA, Casamitjana J, Chang L, Zhang L, James AW, Peault B. Pericytes for Therapeutic Bone Repair. Adv Exp Med Biol. 2018;1109:21–32. Epub 2018/12/14. [PubMed: 30523587]

42. Kraft CT, Agarwal S, Ranganathan K, Wong VW, Loder S, Li J, et al. Trauma-induced heterotopic bone formation and the role of the immune system: A review. J Trauma Acute Care Surg. Jan 2016;80(1):156–65. Epub 2015/10/23. [PubMed: 26491794]

43. Hashimoto K, Kaito T, Furuya M, Seno S, Okuzaki D, Kikuta J, et al. In vivo dynamic analysis of BMP-2-induced ectopic bone formation. Sci Rep. Mar 16 2020;10(1):4751. Epub 2020/03/18. [PubMed: 32179857]

44. Day TF, Guo X, Garrett-Beal L, Yang Y. Wnt/beta-catenin signaling in mesenchymal progenitors controls osteoblast and chondrocyte differentiation during vertebrate skeletogenesis. Dev Cell. May 2005;8(5):739–50. Epub 2005/05/04. [PubMed: 15866164]

45. Wu CL, Dicks A, Steward N, Tang R, Katz DB, Choi YR, et al. Single cell transcriptomic analysis of human pluripotent stem cell chondrogenesis. Nat Commun. Jan 13 2021;12(1):362. Epub 2021/01/15. [PubMed: 33441552]
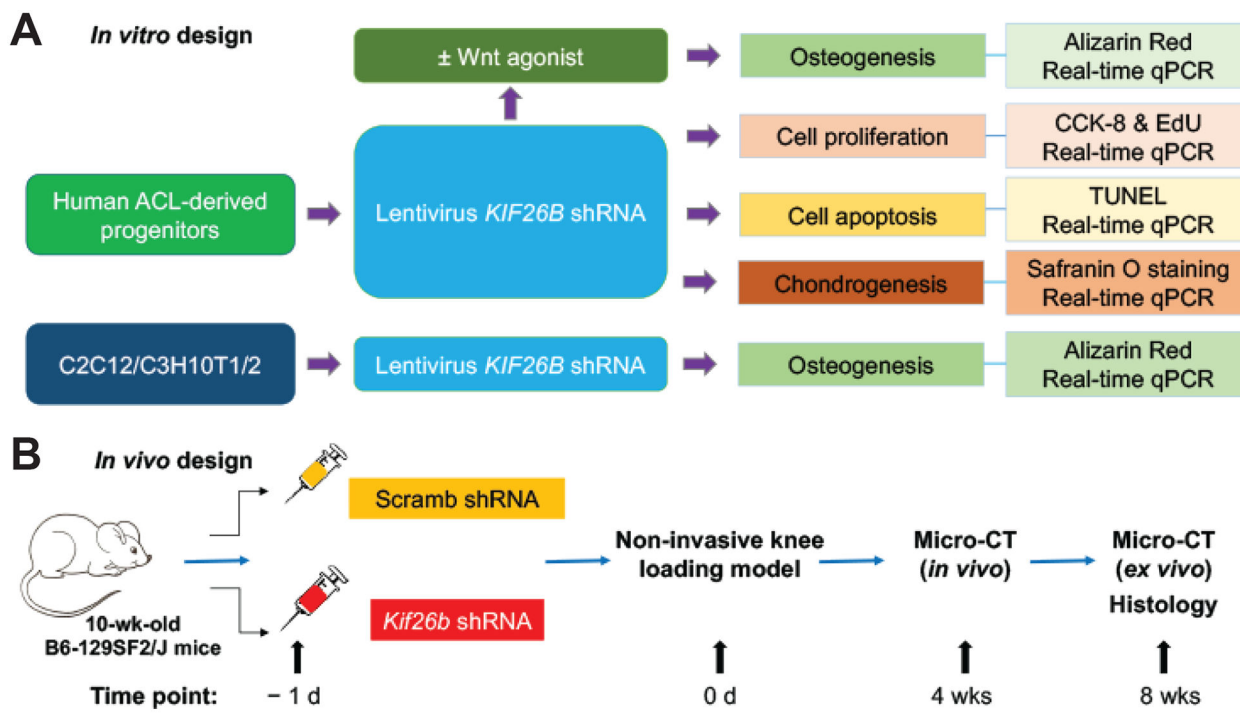
Figure 1:

Study design. **A.** *In vitro* studies were performed using human ACLp cells, murine C2C12 or C3H10T1/2 cells. Cells were transduced with a scrambled shRNA or KIF26B shRNA. Osteogenesis was induced by osteogenesis differentiation medium in all cell types. Osteogenesis was detected by Alizarin red staining and the expression of osteogenic marker genes was measured by RT-qPCR. Chondrogenesis was induced by chondrogenic medium in ACLp cells in a pellet culture system. Successful chondrogenesis was ascertained by measuring the expression of chondrogenic marker genes and Safranin-O staining. Mechanistic role of *KIF26B* knockdown was studied in osteogenic differentiation of ACLp cells in the presence and absence of Wnt agonist II, SKL2001. Cell proliferation was studied by CCK-8 assay and EdU staining while apoptosis was detected by TUNEL. **B.** *In vivo* experiments were conducted in male B6–129SF2/J mice. Mice received either scrambled shRNA or Kif26b shRNA injection in the knee joint after which knees were subjected to non-invasive mechanical loading to instigate intra-articular ectopic calcification. Ectopic calcification was analyzed at 4- and 8-weeks post-loading using micro-CT. Histology was performed to visualize and stain the nodules with Safranin O staining.
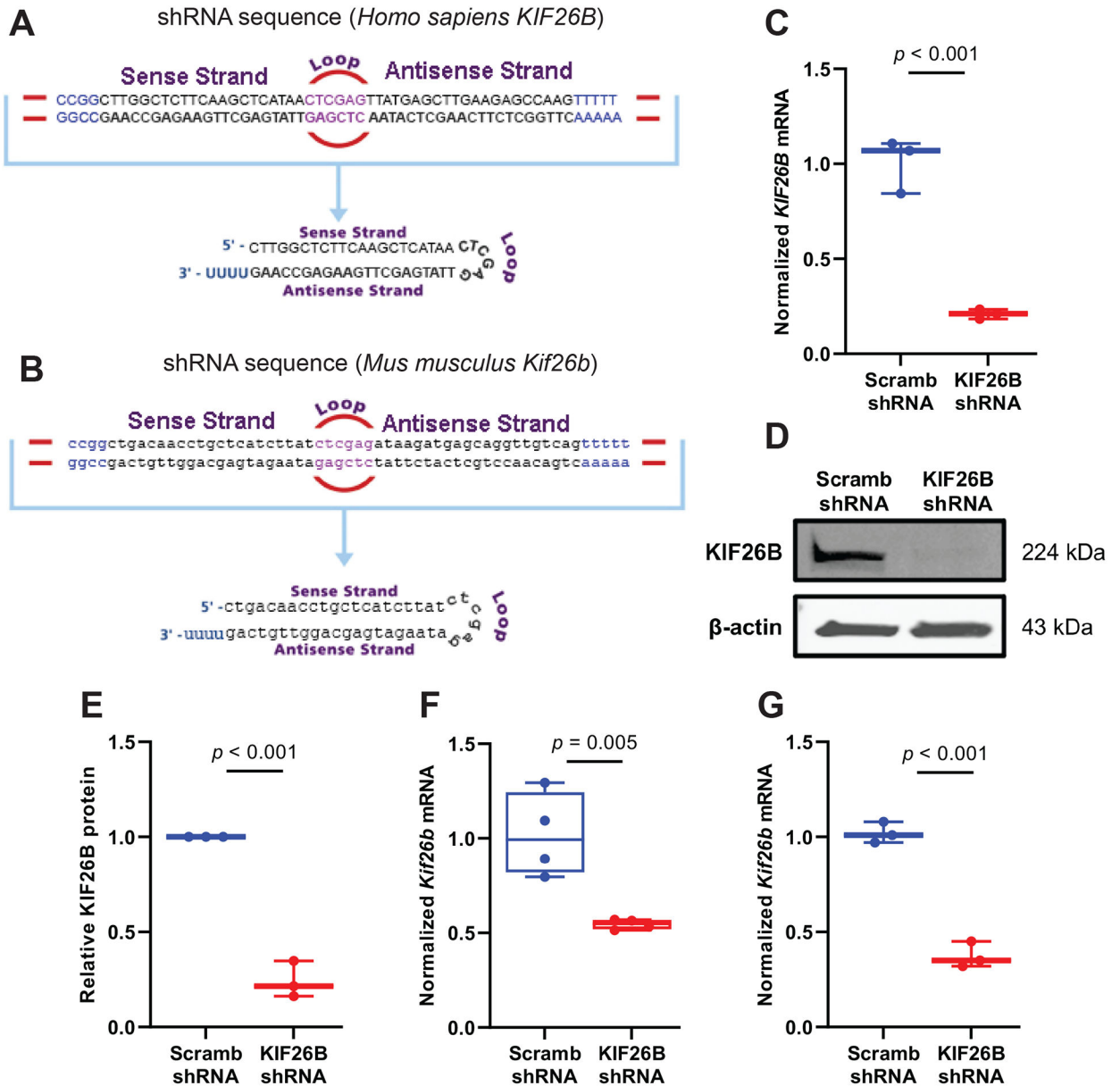
Figure 2: Construction and characterization of lentivirus KIF26B shRNA.
A-B. Human |A| and mouse |B| shRNA sequences targeting KIF26B are shown. **C.** *KIF26B* mRNA expression was significantly decreased in ACLp ($n = 3$) cells transduced with KIF26B shRNA compared with scrambled shRNA at 24-hour time point (Mann-Whitney test). **D.** After 72 hours of transduction with scrambled shRNA or KIF26B shRNA, KIF26B protein was also reduced in ACLp cells ($n = 3$) treated with KIF26B shRNA compared with scrambled shRNA as shown by representative blots. **E.** Quantification of Western blot signal intensity revealed that KIF26B protein expression was significantly less in cells treated with KIF26B shRNA compared with those transduced with scrambled shRNA (Unpaired t-test). **F-G.** After 24 hours of transduction with Kif26b shRNA or scrambled shRNA, *Kif26b* mRNA expression was significantly decreased in C3H10T1/2 ($n = 4$) |F| and C2C12 cells (n
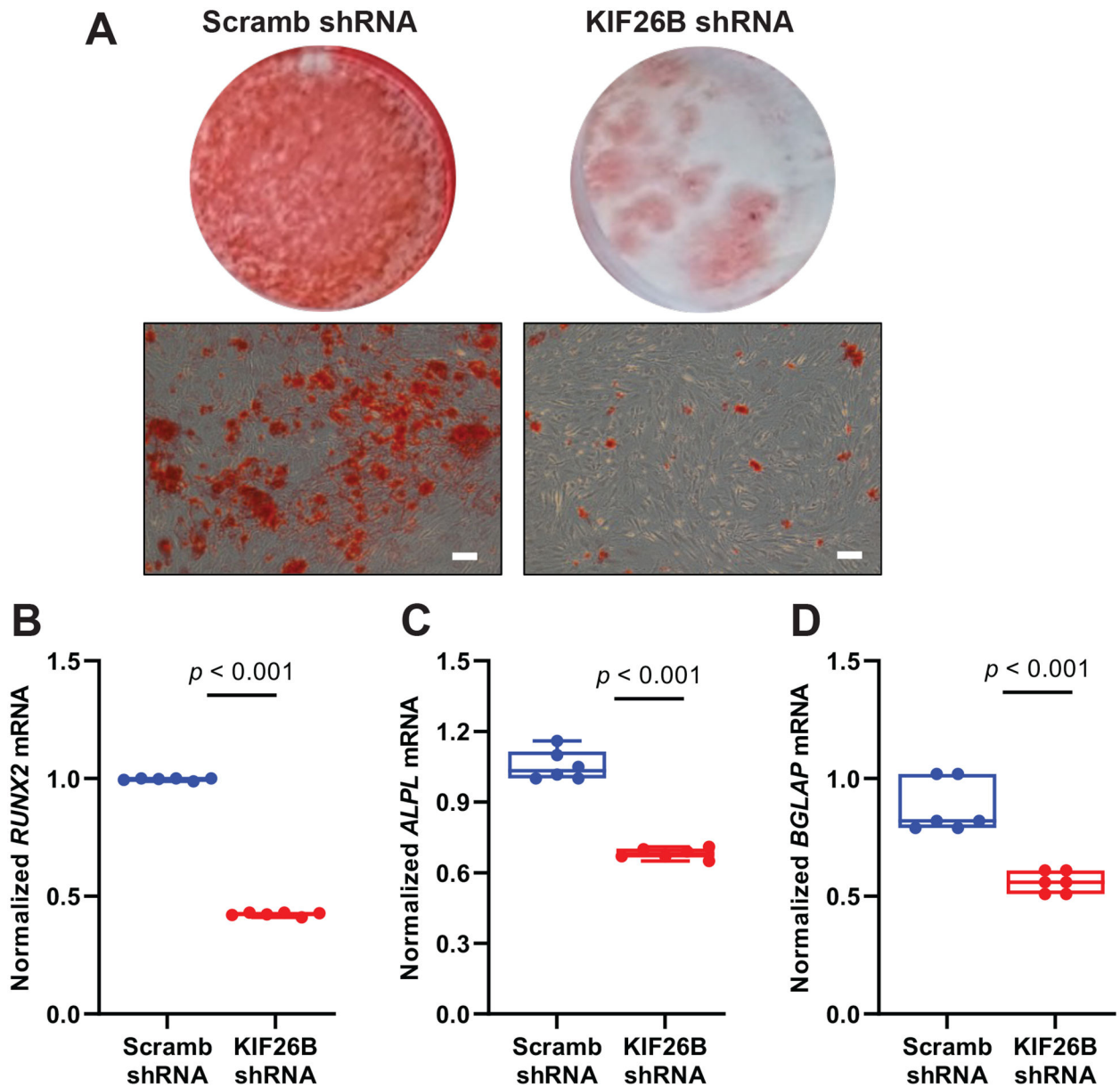
= 3) |G| transduced with Kif26b shRNA compared with scrambled shRNA (Mann-Whitney test).
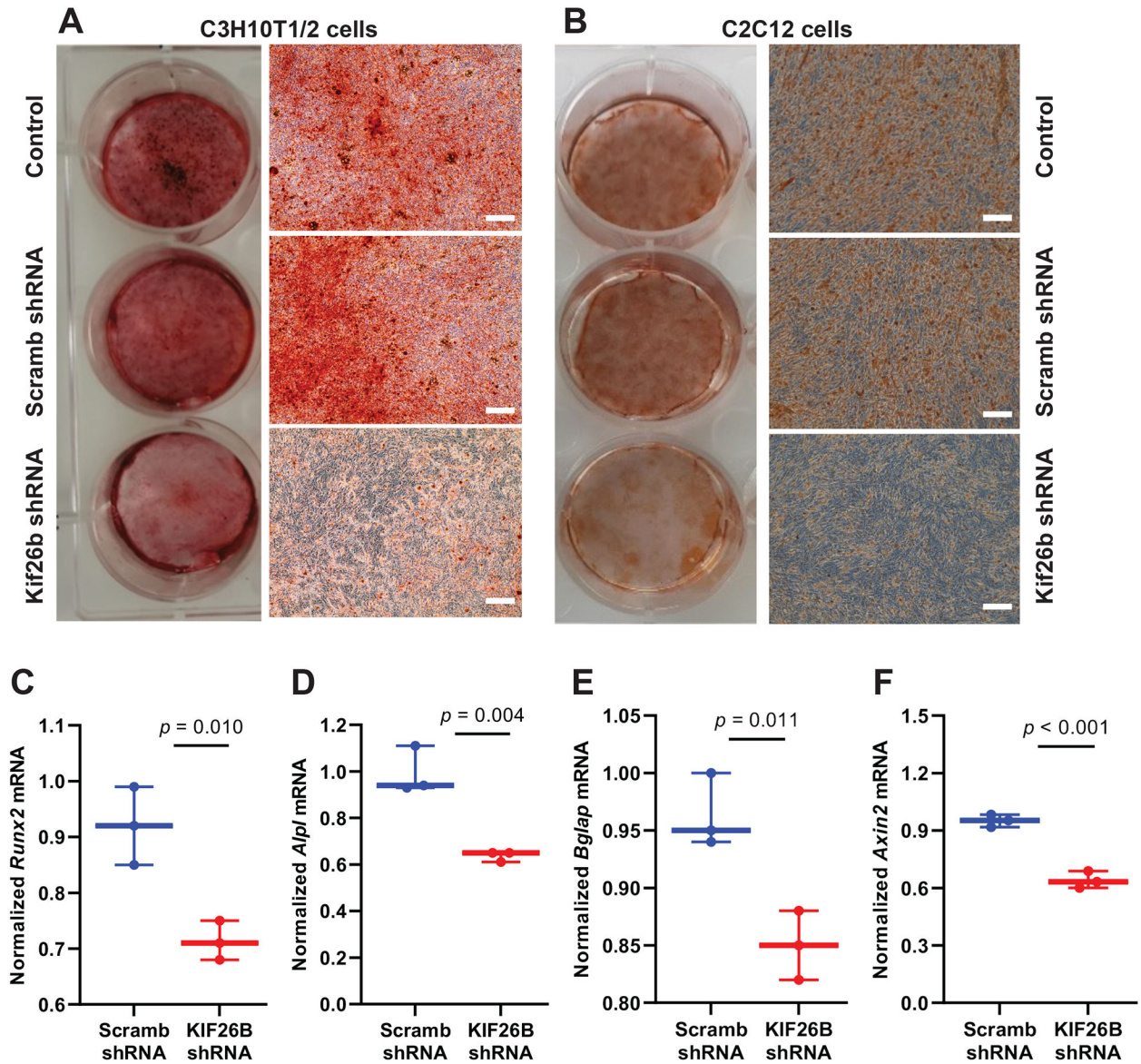
Figure 3: KIF26B silencing attenuates osteogenesis in ACLp cells.
A. KIF26B knockdown significantly arrested matrix mineralization of ACLp cells ($n =$ 6) compared to scrambled shRNA as shown by macro and microphotographs of Alizarin red-stained cells (scale bar = 100 μm). **B-D.** mRNA expression of typical osteogenic marker genes namely *RUNX2* |B|, *ALPL* |C|, and *BGLAP*|D| was significantly decreased in cells transduced with KIF26B shRNA ($n = 6$) compared with those transduced with scrambled shRNA ($n = 6$) (Mann-Whitney test).

Figure 4: KIF26B silencing attenuates osteogenesis in C3H10T1/2 and C2C12 cells.
A-B. Kif26b knockdown significantly arrested matrix mineralization of C3H10T1/2 cells (n = 3) |A| and C2C12 cells (n = 3) |A| compared to scrambled shRNA as shown by macro and microphotographs of Alizarin red-stained cells (scale bar = 200 μm). **C-F.** mRNA expression of typical osteogenic marker genes namely *Runx2* |C|, *Alpl* |D|, and *Bglap* |E| as well as *AXIN2* |F| was significantly decreased in C2C12 cells (n = 3) transduced with KIF26B shRNA compared with those transduced with scrambled shRNA (Mann-Whitney test).
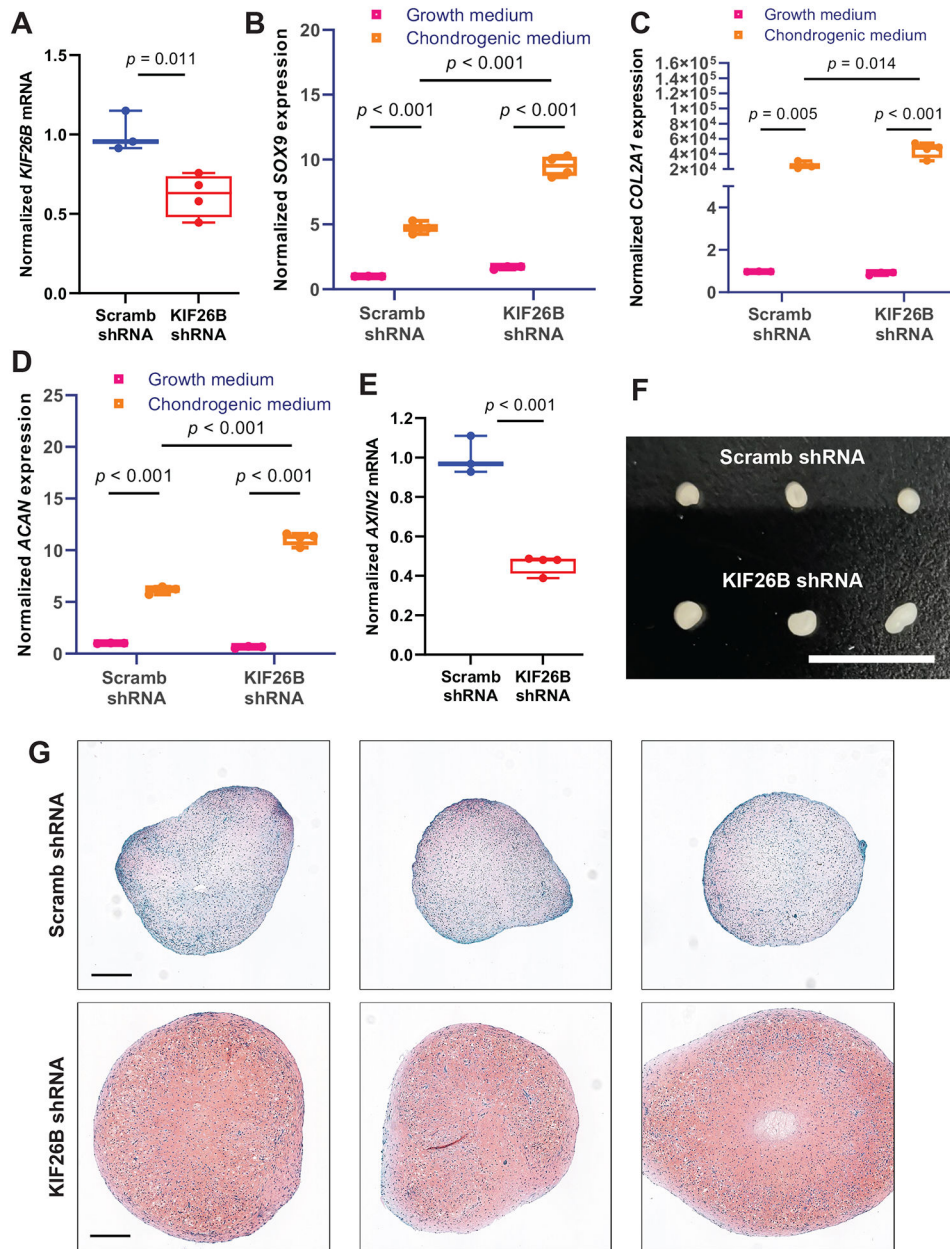
Figure 5: KIF26B knockdown resulted in enhanced chondrogenesis in ACLp cells.
A. *KIF26B* mRNA expression was significantly decreased in pellets prepared from ACLp cells ($n = 3–4$) transduced with KIF26B shRNA compared with scrambled shRNA (Mann-Whitney **B-D.** mRNA expression of typical chondrogenic marker genes namely *SOX9* |B|, *COL2A1* |C|, and *ACAN* |D| was significantly increased in pellets ($n = 3–4$) with cells transduced with KIF26B shRNA than scrambled shRNA in both growth medium and chondrogenic medium. mRNA levels of *SOX9, COL2A1*, and *ACAN* in pellets were both significantly increased in chondrogenic medium compared to those in growth medium, regardless of whether cells were transduced with KIF26B shRNA or scrambled shRNA (2-way ANOVA with Šídák's multiple comparison test). **E.** mRNA expression of *AXIN2* was significantly increased in pellet cultures ($n = 3–4$) transduced with KIF26B shRNA
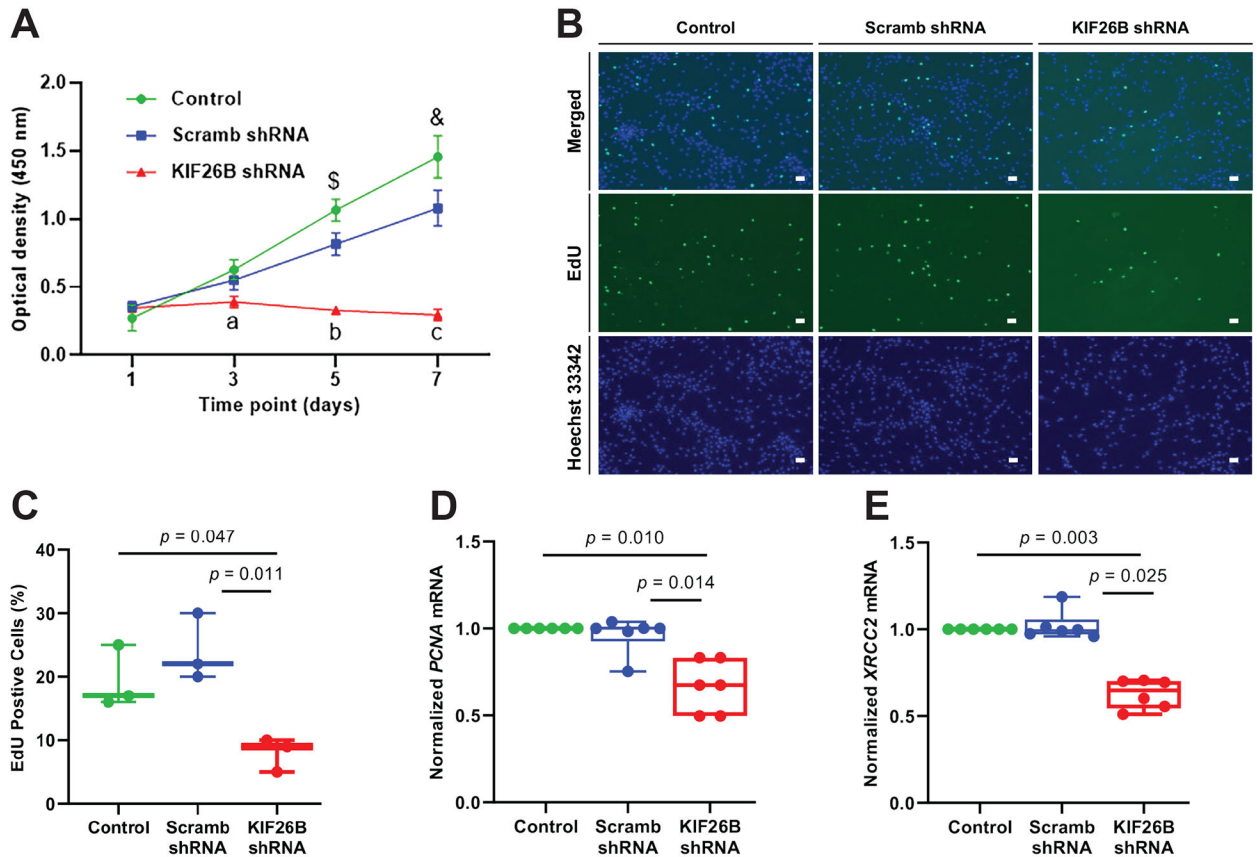
compared with those transduced with scrambled shRNA (Mann-Whitney test). **F.** Size of the pellets was bigger in cells transduced with KIF26B shRNA than scrambled shRNA ($n = 3$ each) (scale bar = 1 cm). **G.** Safranin-O staining of histological sections of pellets showed more intense staining in KIF26B shRNA group than scrambled shRNA group ($n = 3$ each).

Figure 6: Loss of KIF26B decreases number of living cells and proliferation.
A. *KIF26B* knockdown significantly reduced number of living ACLp cells ($n = 4$) compared with scrambled shRNA and untreated control groups as determined by CCK-8 assay. \$ and &: statistically significance differences between scrambled shRNA and control groups with $p = 0.011$ and $p = 0.025$, respectively; a, b, and c: statistically significant differences between scrambled shRNA and KIF26B shRNA groups with all $p < 0.05$ (2-way ANOVA with Šídák's multiple comparison test). **B.** After 72 hours of transduction with scrambled shRNA or *KIF26B* shRNA, EdU incorporation assay for measuring cell proliferation showed that KIF26B knockdown decreased the numbers of EdU positive cells as displayed in immunofluorescence images ($n = 3$ each). Blue = Hoechst 3342; Green = EdU, scale bar = 100 μm. **C.** Quantification of cell numbers revealed significantly reduced the fraction of EdU positive cells compared to both untreated control and scrambled shRNA groups (1-way analysis of variance with Tukey's post hoc test). **D-E.** mRNA expression of cell proliferation markers namely *PCNA* |D|, *XRCC2* |E| was significantly decreased in cells treated with KIF26B shRNA ($n = 6$) and compared to both untreated control and scrambled shRNA groups ($n = 6$ each) (Kruskal-Wallis with Dunn's multiple comparison test).
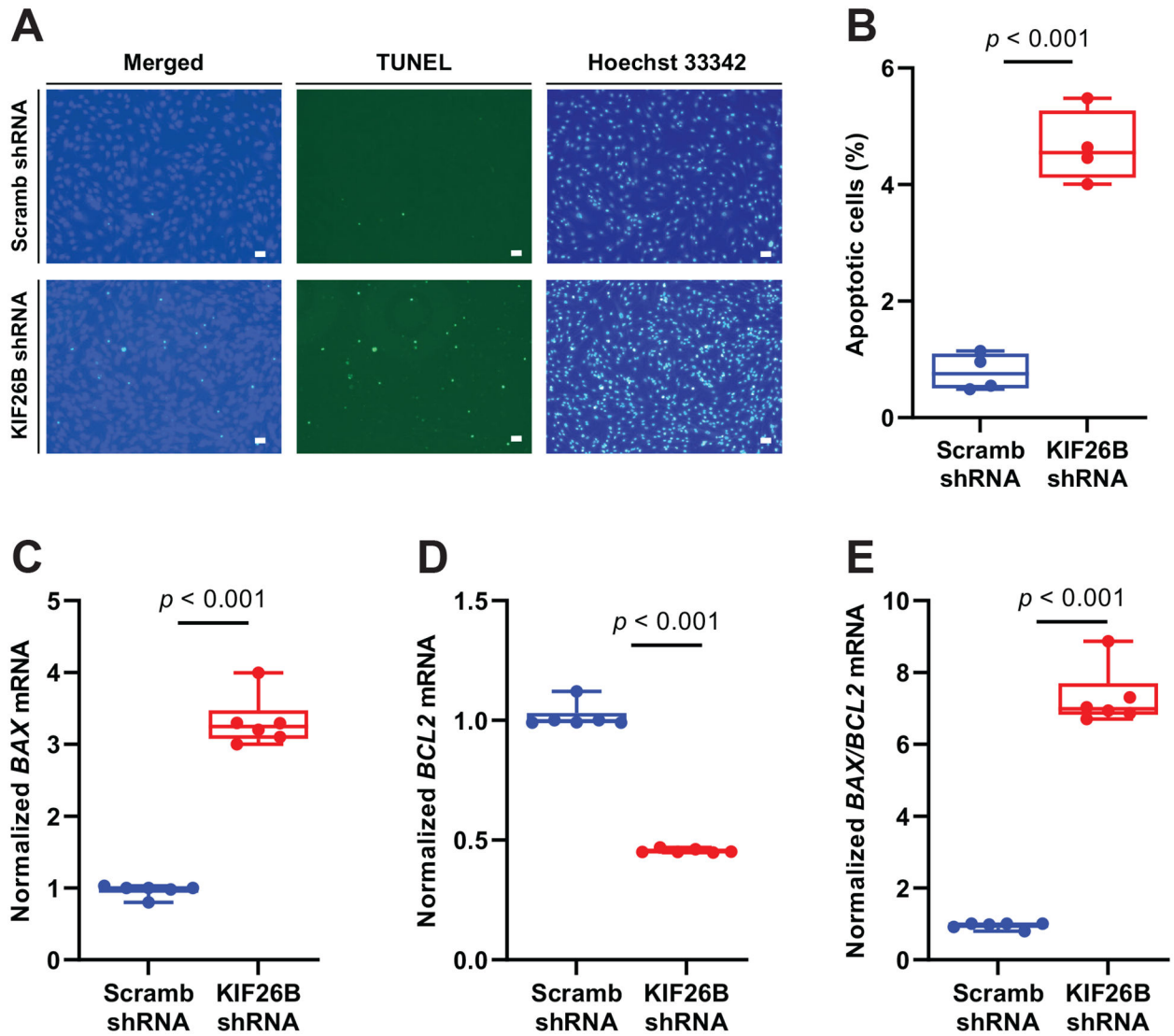
Figure 7: Loss of *KIF26B* induces cellular apoptosis.

A. After 72 hours of transduction with scrambled shRNA or KIF26B shRNA, KIF26B knockdown increased the number of TUNEL positive cells as measured by TUNEL assay compared to scrambled shRNA group ($n = 4$ each). Blue = Hoechst 3342; Green = TUNEL, scale bar = 100 μm. **B.** Quantification revealed that percentage of TUNEL positive cells was significantly higher in KIF26B shRNA group compared to scrambled shRNA group (Unpaired t-test). **C-E.** mRNA expression of pro-apoptotic gene *BAX* |C| was significantly higher in cells treated with KIF26B shRNA compared to scrambled shRNA group while mRNA expression of anti-apoptotic gene *BCL2* |D| was significantly lower in cells treated with KIF26B shRNA. *BAX/BCL2* ratio |E| was significantly higher in cells treated with KIF26B shRNA than those treated with scrambled shRNA ($n = 6$ each) (Mann-Whitney test).
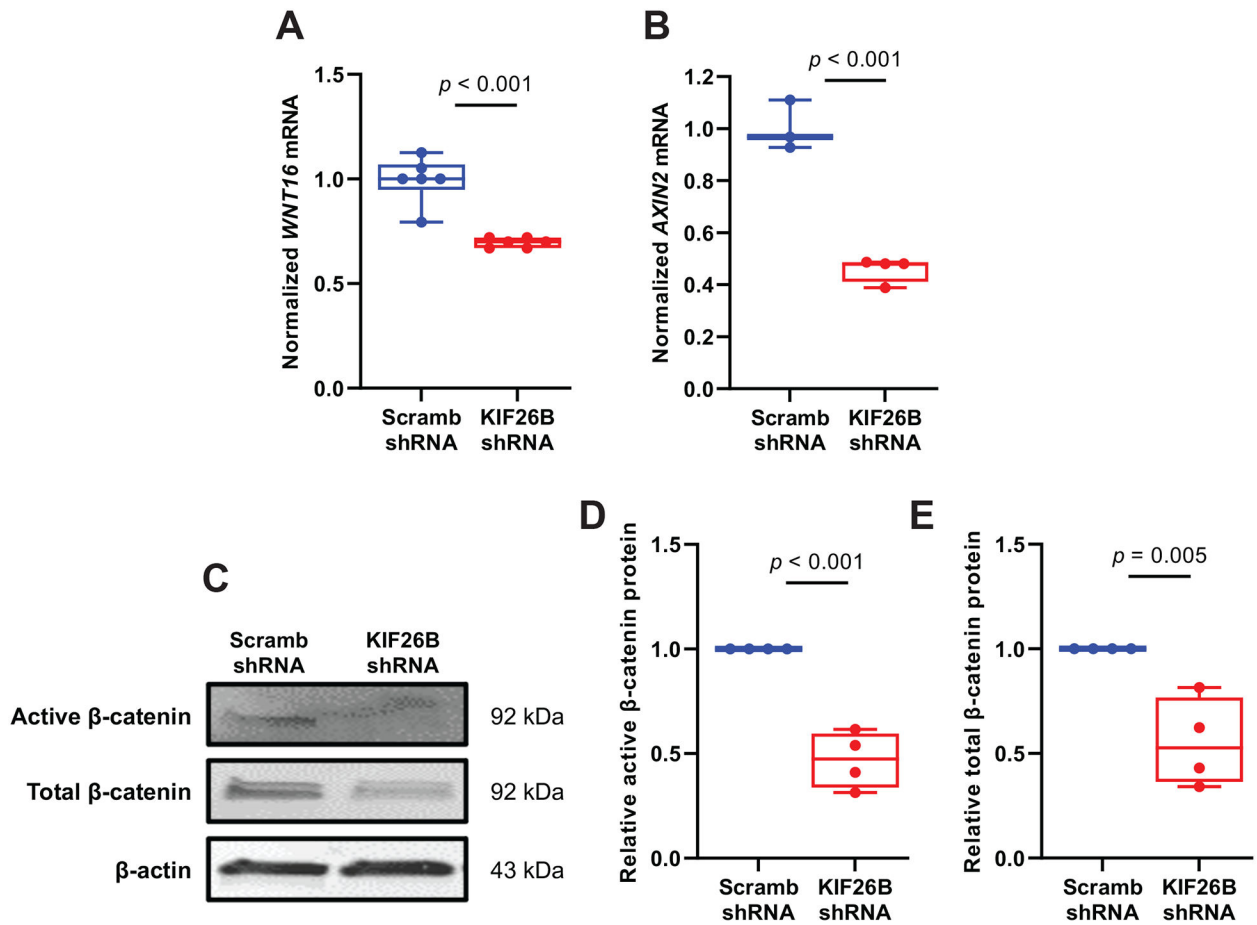
Figure 8: Modulation of canonical Wnt/β-catenin signaling by KIF26B.
A-B. KIF26B knockdown suppressed mRNA expression of Wnt//β-catenin pathway genes namely *WNT16* |A| and *AXIN2* |B| compared with scrambled shRNA ($n = 6$ each) (Mann-Whitney test). **C.** After 7 days of osteogenic induction, representative Western blot images showed the expression of non-phosphorylated (active) β-catenin at Ser33/37/Thr41 and total β-catenin in ACLp cells ($n = 4$) transduced with either KIF26B shRNA or scrambled shRNA. **D-E.** Quantification of Western blot signaling intensity revealed that both active β-catenin |D| and total β-catenin |E| were significantly lower in KIF26B shRNA group compared to scrambled shRNA group (Unpaired t-test).
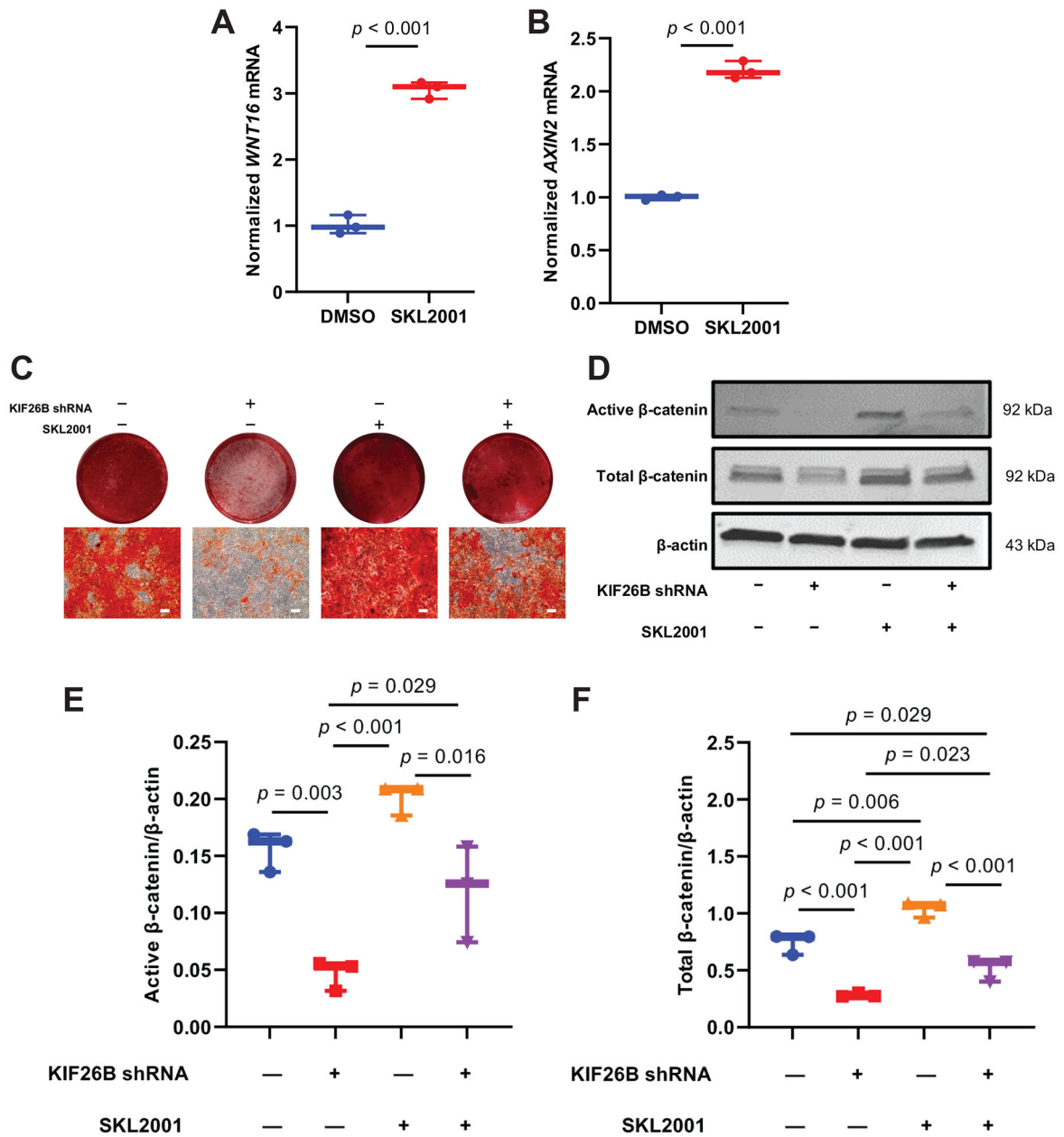
Figure 9: Wnt agonist rescued loss of osteogenesis due to KIF26B knockdown.
A-B. The expression of *WNT16* |A| and *AXIN2* |B| mRNA was increased significantly in ACLp cells treated with SKL2001 compared with vehicle (DMSO) ($n = 3$ each, Mann-Whitney test). **C.** Addition of Wnt agonist SKL2001 reversed osteogenesis suppression by *KIF26B* loss-of-function in cells transduced with KIF26B shRNA as shown by macro and micrographs of cells stained with Alizarin red ($n = 3$ each, scale bar = 100 μm). **D.** After 7 days of osteogenic induction, the protein levels of active and total β-catenin lost due to *KIF26B* were also regained with SKL2001 treatment ($n = 3$ each). **E-F.** Quantification of signal intensity of active β-catenin |E| and total β-catenin |F| confirmed the expression pattern of active and total β-catenin (1-way ANOVA with Tukey's post hoc test).
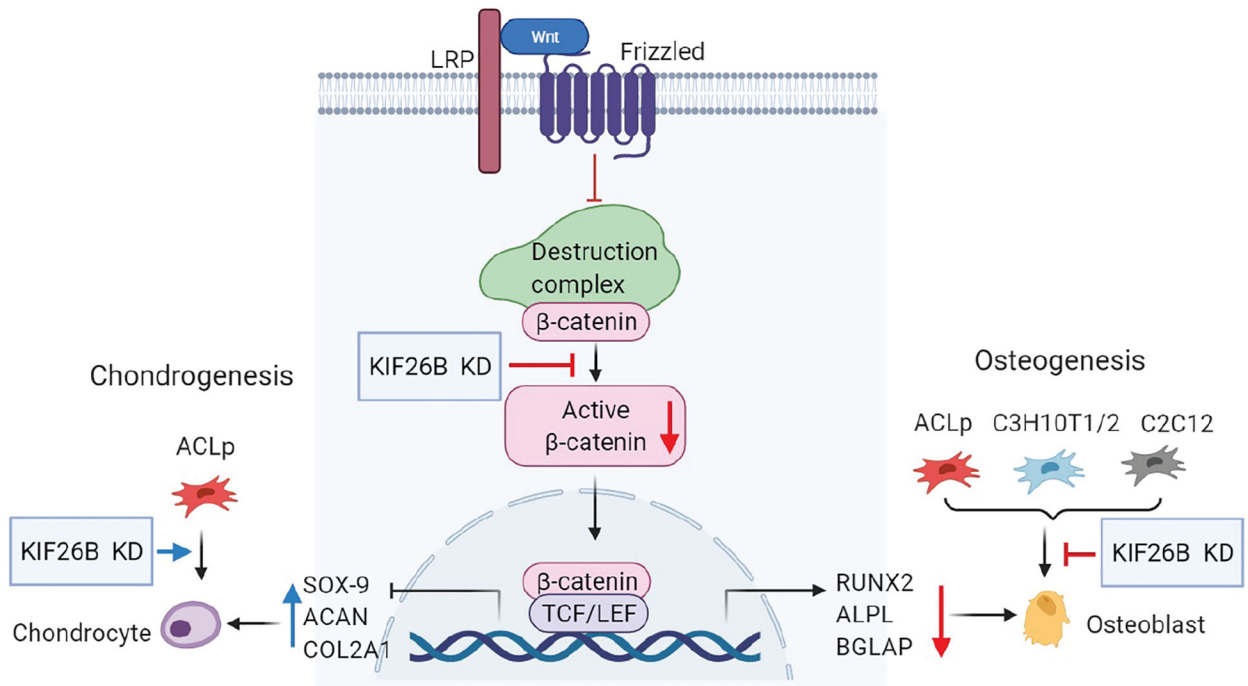
Figure 10: Schematic of proposed mechanism of KIF26B in ectopic calcification and its interaction with Wnt/β-catenin signaling.

KIF26B inhibition decreases β-catenin levels by increasing the degradation of β-catenin. It resulted in suppression of osteogenesis and the expression of typical osteogenic-specific marker genes; and elevation of chondrogenesis as well as elevation of chondrogenic-specific marker genes.
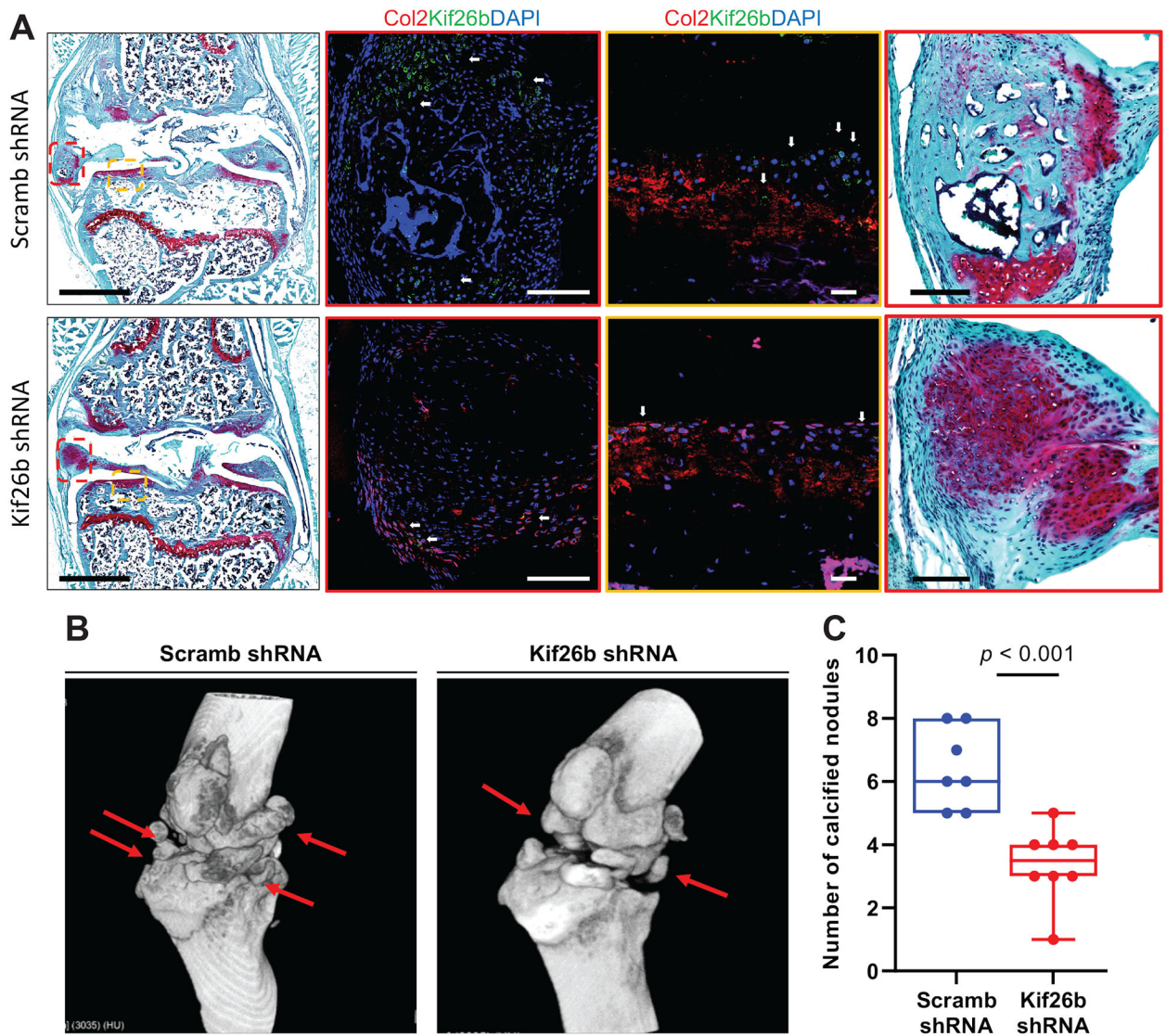
Figure 11: Kif26b shRNA prompted chondrogenesis and inhibited ectopic calcification in mice.
A. Representative low magnification histology images (scale bar = 1 mm) are shown for scrambled and Kif26b shRNA groups to provide an overview of the knee joint and ectopic nodule. Confocal microscopy images of Kif26b immunostaining (white arrowhead) in the calcified nodule (red square) or cartilage area (orange square) showing decreased staining intensity of Kif26b in Kif26b shRNA group indicative of successful Kif26b knockdown *in vivo* (green = Kif26b, red = Col 2, blue = DAPI, Scale bars = 100 μm). In addition, Safranin O staining of nodules showed increased staining intensity in Kif26b shRNA group compared with the scrambled shRNA group (Scale bar = 100 μm) (n = 3 each). **B.** Representative μCT images at 8 weeks are shown demonstrating less calcified nodules in mice receiving Kif26b shRNA (n = 8) compared with those receiving scrambled shRNA (n = 7) (red arrows point to nodules) **C.** Quantification of calcified nodules showed that number of calcified nodules were significantly lower in mice treated with Kif26b shRNA than those treated with shRNA at 8 weeks (Unpaired t-test).

Table 1:

Characteristics of patients from which ACL progenitor cells were collected and analyzed

Patient No.	Age (year)	Sex	Experiment	Data in
P15-063	15	Female	RT-qPCR	Fig. 2C
P15-064	19	Male	RT-qPCR	Fig. 2C
P15-065	16	Male	RT-qPCR	Fig. 2C
P15-066	13	Female	Western blot	Fig. 2D–E
P15-067	16	Female	Western blot	Fig. 2D–E
P15-068	47	Male	Western blot	Fig. 2D–E
P15-031	15	Female	Cell egression	S. Fig. 1A
P15-032	34	Female	Cell egression	S. Fig. 1A
P15-033	25	Male	Cell egression	S. Fig. 1A
P15-070	21	Female	Immunostaining, ARS	S. Fig. 1B–C
P15-071	18	Male	Immunostaining, ARS	S. Fig. 1 B–C
P15-072	19	Female	Immunostaining, ARS	S. Fig. 1B–C
P15-069	40	Female	ARS, RT-qPCR	S. Fig. 1D
P15-073	19	Female	ARS, RT-qPCR	S. Fig. 1D
P15-075	50	Male	ARS, RT-qPCR	S. Fig. 1D
P15-077	19	Female	ARS, RT-qPCR	S. Fig. 1D
P15-078	44	Female	ARS, RT-qPCR	S. Fig. 1D
P15-079	60	Female	ARS, RT-qPCR	S. Fig. 1D
P15-080	33	Female	ARS, RT-qPCR	Fig. 3A–D
P15-081	23	Male	ARS, RT-qPCR	Fig. 3A–D
P15-082	17	Male	ARS, RT-qPCR	Fig. 3A–D
P15-083	15	Female	ARS, RT-qPCR	Fig. 3A–D
P15-084	20	Male	RT-qPCR	Fig. 3B–D
P15-085	34	Male	RT-qPCR	Fig. 3B–D
P15-113	46	Male	RT-qPCR	Fig. 5A–E
P15-114	37	Male	RT-qPCR, S-O staining	Fig. 5A–G
P15-086	33	Female	CCK-8, EdU, RT-qPCR	Fig. 6A–E

Patient No.	Age (year)	Sex	Experiment	Data in
P16-115	27	Female	RT-qPCR, S-O staining	Fig. 5A–G
P15-116	39	Male	RT-qPCR, S-O staining	Fig. 5A–G
P15-087	36	Female	CCK-8, EdU, RT-qPCR	Fig. 6A–E
P15-088	14	Male	CCK-8, EdU, RT-qPCR	Fig. 6A–E
P15-089	40	Male	RT-qPCR	Fig. 6D–E
P15-090	25	Male	RT-qPCR	Fig. 6D–E
P15-091	43	Male	RT-qPCR	Fig. 6D–E
P15-092	53	Female	TUNEL, RT-qPCR	Fig. 7A–E
P15-093	45	Male	TUNEL, RT-qPCR	Fig. 7A–E
P15-094	16	Male	TUNEL, RT-qPCR	Fig. 7A–E
P15-095	19	Female	TUNEL, RT-qPCR	Fig. 7A–E
P15-096	18	Female	RT-qPCR	Fig. 7C–E
P15-097	45	Male	RT-qPCR	Fig. 7C–E
P15-098	18	Female	RT-qPCR	Figs. 8A–B, 9A–B
P15-099	21	Male	RT-qPCR	Figs. 8A–B, 9A–B
P15-101	55	Female	RT-qPCR	Figs. 8A–B, 9A–B
P15-102	36	Female	RT-qPCR, Western blot	Fig. 8A–E
P15-103	16	Female	RT-qPCR, Western blot	Fig. 8A–E
P15-104	22	Female	RT-qPCR, Western blot	Fig. 8A–E
P15-105	23	Female	Western blot	Fig. 8C–E
P15-106	40	Female	ARS	Fig. 9C
P15-107	16	Female	ARS	Fig. 9C
P15-108	16	Female	ARS	Fig. 9C
P15-110	30	Female	Western blot	Fig. 9D–F
P15-111	16	Male	Western blot	Fig. 9D–F
P15-112	16	Female	Western blot	Fig. 9D–F
			-	

Author Manuscript

Author Manuscript

Author Manuscript

Author Manuscript

ACL = anterior cruciate ligament; RT-qPCR = real-time polymerase chain reaction; ARS = Alizarin red staining; S-O = Safranin-O; CCK-8 = Cell Counting Kit 8; EdU = 5-ethynyl-2′-deoxyuridine; TUNEL= terminal deoxynucleotidyl transferase (TdT)-mediated dUTP nick-end labelling

Table 2:

The characteristics of primers used in this study

Gene symbol	Species	Accession No.	Primer sequence 5'–3' Forward	Primer sequence 5'–3' Reverse	Location	Amplicon size (bp)
KIF26B	*Homo sapiens*	NM_018012.4	CGTGTTCTTCACACTGCACA	TTTCACACAGCTGCCGAGAT	2480–2591	102
ALPL	*Homo sapiens*	NM_000478.5	GACATCGCCTACCAGCTCAT	CCTGGCTTTCTCGTCACTCT	871–993	123
RUNX2	*Homo sapiens*	NM_001278478.1	ACAGTAGATGGACCTCGGGA	GGATGAGGAATGCGCCCTAA	868–974	107
BGLAP	*Homo sapiens*	NM_199173.5	GTAGTGAAGAGACCCAGGCG	TCAGCCAACTCGTCACAGTC	403–524	122
PCNA	*Homo sapiens*	NM_002592.2	AACCTGCAGAGCATGGACTC	ATACTGGTGAGGTTCACGCC	345–463	119
XRCC2	*Homo sapiens*	NM_005431.2	CCTTGCCCGACTTGAAGGTA	TCCTGTTCCTTCTGGGCCAT	104–221	118
BAX	*Homo sapiens*	NM_001291428.2	CTGACGGCAACTTCAACTGG	GTCCAATGTCCAGCCCATGA	356–480	125
BCL2	*Homo sapiens*	NM_000633.2	GGGGAGGATTGTGGCCTTCTT	ATCCACAGGGCGATGTTGTC	926–1023	98
WNT16	*Homo sapiens*	NM_057168.1	CTTTGGCTACGAGCTGAGCA	TCTGTCATGTTGCCTGCACT	581–694	114
AXIN2	*Homo sapiens*	NM_004655.4	TGATGCGCTGACGGATGATT	ATTGGCCTTCACACTGCGAT	1227–1347	121
SOX9	*Homo sapiens*	NM_000346.4	CGAGCCCGATCTGAAGAAGG	CCAGTCGTAGCCTTTGAGCA	540–630	91
COL2A1	*Homo sapiens*	NM_001844.4	CCCAGAGGTGACAAAGGAGA	CACCTTGGTCTCCAGAAGGA	3521–3619	117
ACAN	*Homo sapiens*	NM_001135.4	GGCACTAGTCAAACCCTTTGG	CTGAACCCTGGTAACCCTGA	5704–5779	95
PPIA	*Homo sapiens*	NM_021130.4	CTGCACTGCCAAGACTGAG	TGGTCTTTGCCATTCCTGGAC	430–546	117
Kif26b	*Mus musculus*	NM_0011611665.1	ctcaactcggtggccattca	ggtctcgtcatcagctggg	1348–1461	114
Runx2	*Mus musculus*	NM_001146038.2	ccacctctgacttctgcctc	gaactgcctgggggtctgaaa	1292–1386	95
Bglap2	*Mus musculus*	NM_001032298.3	gtccaagcaggagggcaata	ttaagctcaactgctcccg	156–263	108
Alpl	*Mus musculus*	NM_007431.3	ctgactgacccttcgtctc	ggtcaatcctgcctccttcc	1153–1255	103
Axin2	*Mus musculus*	NM_015732.4	gaccgacgattccatgtcca	attggccttcacactgcgat	1270–1381	112
Gapdh	*Mus musculus*	NM_001289726.1	aggtcggtgtgaacggatttg	tgtagaccatgtagttgaggtca	100–222	123

bp = base pair